Geological Society, London, Special Publications

The Java convergent margin: structure, seismogenesis and subduction processes

Heidrun Kopp

Geological Society, London, Special Publications 2011; v. 355; p. 111-137 doi: 10.1144/SP355.6

Email alerting

service

click here to receive free e-mail alerts when new

articles cite this article

Permission request

click here to seek permission to re-use all or part of

this article

Subscribe

click here to subscribe to Geological Society, London, Special Publications or the Lyell Collection

Notes

Downloaded by on August 5, 2011



The Java convergent margin: structure, seismogenesis and subduction processes

HEIDRUN KOPP

IFM-GEOMAR Leibniz-Institute of Marine Sciences, Wischhofstr. 1-3, 24148 Kiel, Germany (e-mail: hkopp@ifm-geomar.de)

Abstract: The Java margin is characterized by a distinct variation in lower to upper plate material transfer and recurring catastrophic tsunamogenic earthquakes. Both processes are closely linked to the subduction of oceanic basement relief resulting in varying degrees of fore-arc deformation. Tomographic models of refraction seismic profiles and reflection seismic lines in combination with high-resolution multibeam bathymetric data reveal the variability in the deep structure and deformation of the Java fore-arc. Shallow subduction processes are governed by the sediment supply in the trench as well as by the nature and fabric of the oceanic lithosphere. The deep structure of the fore-arc reveals a shallow upper plate crust—mantle transition, present along the entire Java margin section. The serpentinized fore-arc mantle wedge governs the depth extent of the seismogenic zone here, which is narrower compared to its Sumatran analogue. In addition, offshore central Java, high relief oceanic basement features potentially act as asperities as well as barriers to seismic rupture, limiting the possible magnitude of subduction thrust earthquakes. However, the potential for geohazards, in particular tsunamis, is high along the entire margin. This results from tsunamogenic earthquakes, ubiquitous splay faults and potentially tsunamogenic landslides, which further increase the risk of future tsunamis.

This contribution reviews studies of the Java subduction zone (Fig. 1) with a special emphasis on the neotectonic processes and structural evolution of the fore-arc using tomographic images based on seismic refraction data (Fig. 2) and multibeam bathymetry (Fig. 3). Following introductory remarks on the tectonic setting, seismicity and geophysical data base, the observational and interpretative information gained from these studies will be presented area-specific for each tectonic segment along the margin. Going from west to east, these first-order segments are defined based on the dominating material transfer and nature of the lower plate, that is sediment accretion offshore Sunda Strait and western Java, fore-arc erosion offshore central-eastern Java, and continent-island arc collision offshore Sumba Island. A regional summary is presented in the conclusions.

Tectonic setting

The Java trench forms the eastern section of the Sunda deep-sea trench and is the site where the Indo-Australian oceanic lithosphere subducts beneath the Sundaland block of Indonesia. It straddles the island of Java and the Lesser Sunda islands of Bali, Lombok and Sumbawa (Fig. 1). The Java margin is bound in the west by the transtensional regime of the southern Sunda Strait (Lelgemann *et al.* 2000). The Sunda Strait marks the hinge line and passage from the trench-perpendicular

convergence off Java to the oblique subduction offshore Sumatra. In the east, the Java trench terminates at 121°E where it merges into the Timor trough (Audley-Charles 1975, 2004; Hall & Smyth 2008). The transition from oceanic subduction along the Java trench to continent–island arc collision along the Timor trough of the Banda arc occurs south of Sumba Island, where continental crust is colliding with the fore-arc (Hamilton 1979) (Fig. 1).

The Indo-Australian plate currently moves at $6.7 \, \mathrm{cm/a}$ in a direction N11°E off western Java and thus almost normal to the trench (Tregoning *et al.* 1994) (Fig. 1). Convergence speed slightly increases from western Java towards the east, however, at a very subtle rate, reaching $c. 7 \, \mathrm{cm/a}$ off Bali (Simons *et al.* 2007) and has been active since the Eocene (Hall & Smyth 2008). A local source tomography based on recordings over a period of almost six months from more than 100 seismic stations on Java images the steep dip angle of the subducting slab, reaching $c. 70^{\circ}$ underneath the island (Koulakov *et al.* 2007).

The age of the incoming plate increases from Late Cretaceous offshore Sunda Strait ($105^{\circ}E$) to Late Jurassic at $120^{\circ}E$. Accordingly, water depth in the trench increases from c. 6 km off the Sunda Strait to more than 7 km off Lombok and Sumbawa in the east and correlates with the decrease in sediment supply from c. 1500 m off western Java to the starved trench segments along the eastern Java trench.

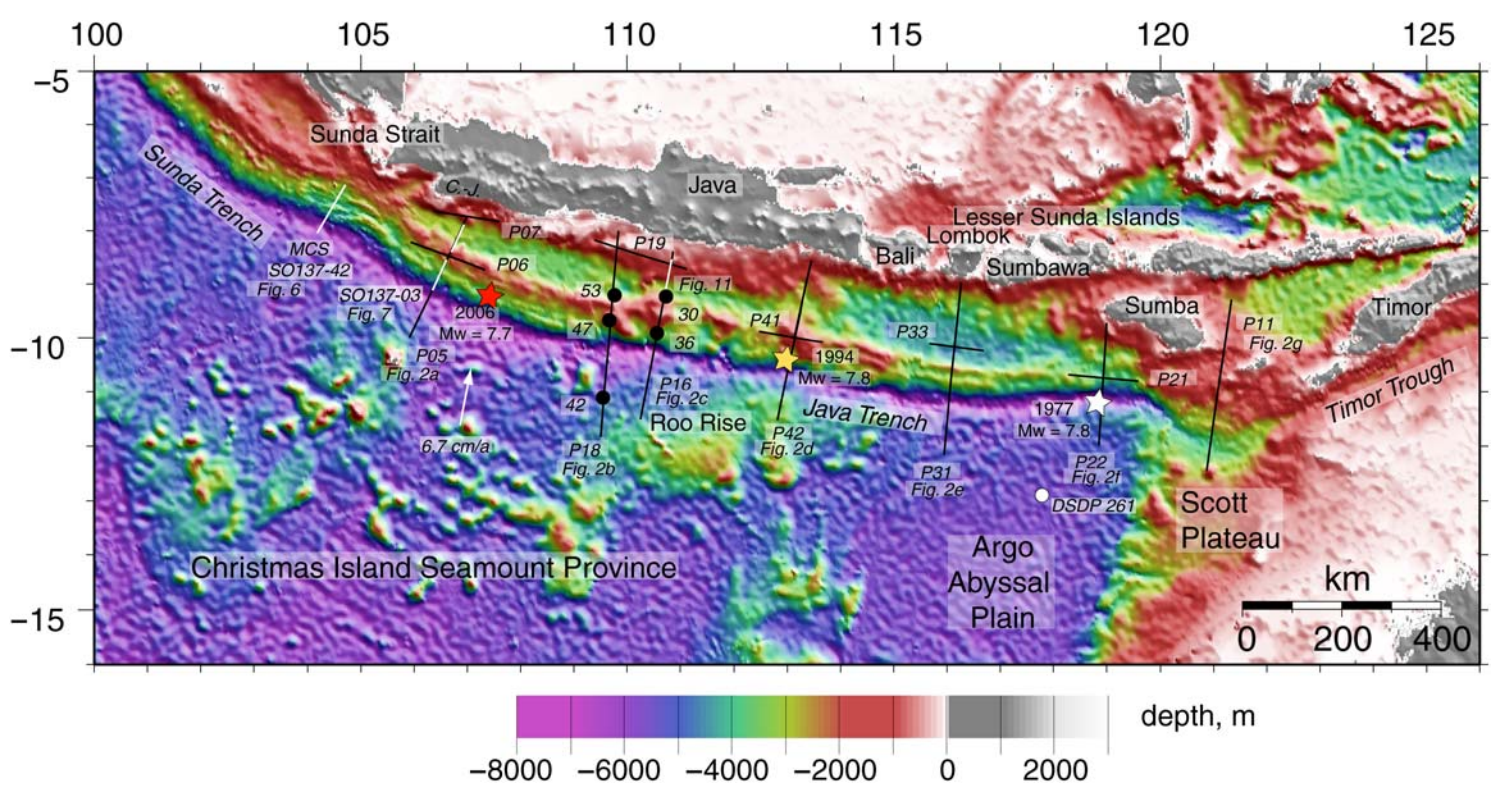


Fig. 1. Morphology of the Java margin based on satellite altimetry data (Smith & Sandwell 1997). A large bivergent accretionary wedge is expressed as a continuous bathymetric ridge fronting the Java fore-arc basin offshore western Java. This ridge structure is broken and highly deformed offshore central Java, where the oceanic Roo Rise is colliding with the margin. The eastern Java trench offshore Bali to Sumba is characterized by the subduction of smooth oceanic crust of the Argo Abyssal Plain. The transition from oceanic subduction to continent—island arc collision occurs south of Sumba where the Scott plateau enters the trench. Black lines show wide-angle refraction profiles. Black dots show locations of ocean bottom instruments displayed in Figures 4, 5, 8, 9 and 12. White lines show extent of MCS data shown in Figures 6, 7 and 11. Stars denote earthquake hypocentres of 1977 (white), 1994 (yellow) and 2006 (red). C.-J.: Ciletuh-Jampang block.

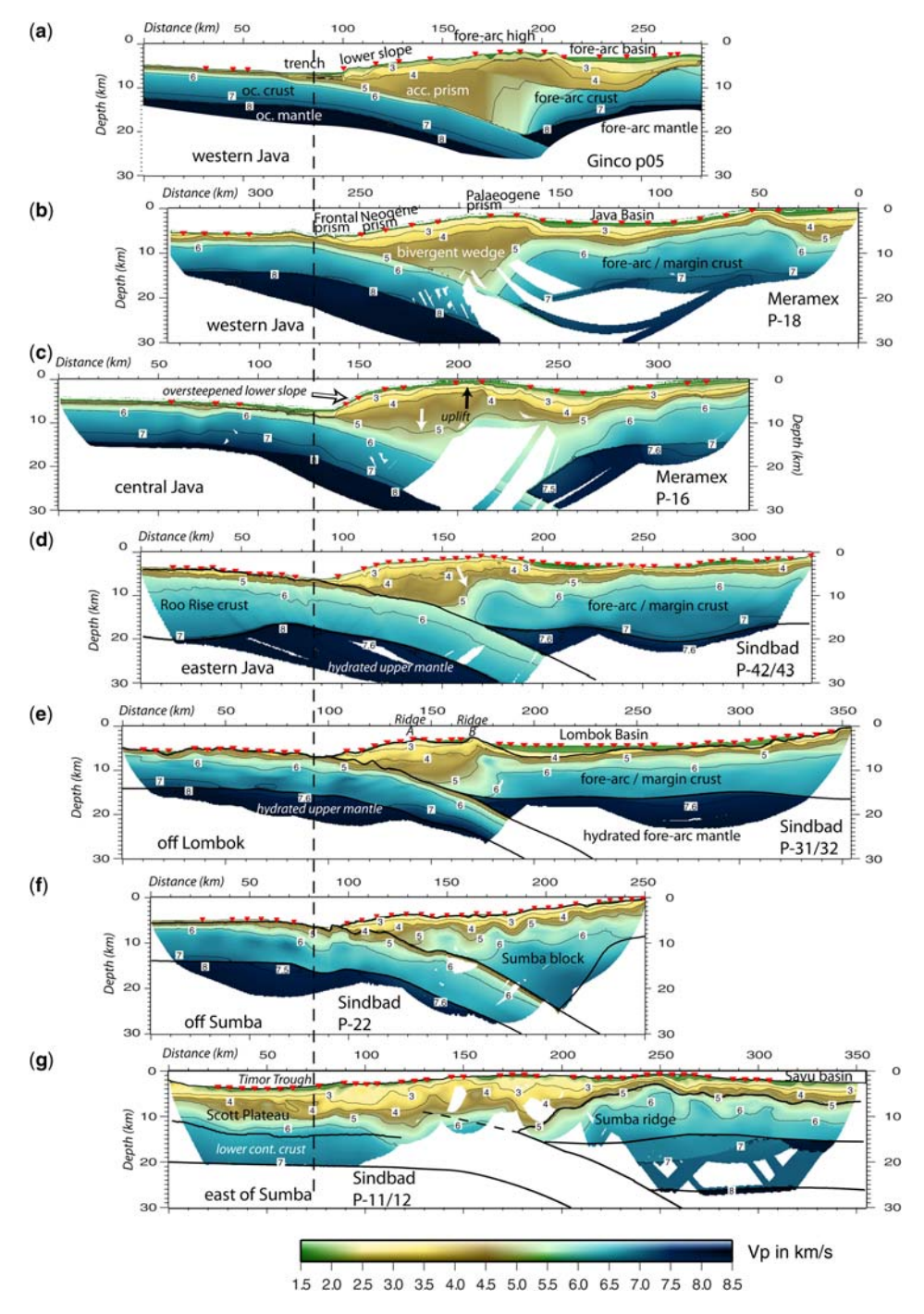


Fig. 2. Tomographic images and velocity—depth distribution along seven refraction seismic dip lines crossing the fore-arc between western Java and east of Sumba island. The profiles document the variation from the accretionary domain (**a** and **b**) to the erosional seamount/plateau subduction regime off central to eastern Java (**c** and **d**). To the east, the transition from oceanic subduction offshore Lombok (**e**) to continent—island arc collision (**f** and **g**) occurs. All profiles west of Sumba show a shallow hydrated upper plate mantle, which limits the downdip extent of the seismogenic zone. Profiles are approximately aligned along the vertical stippled line. Vertical exaggeration in all profiles is 2.5.

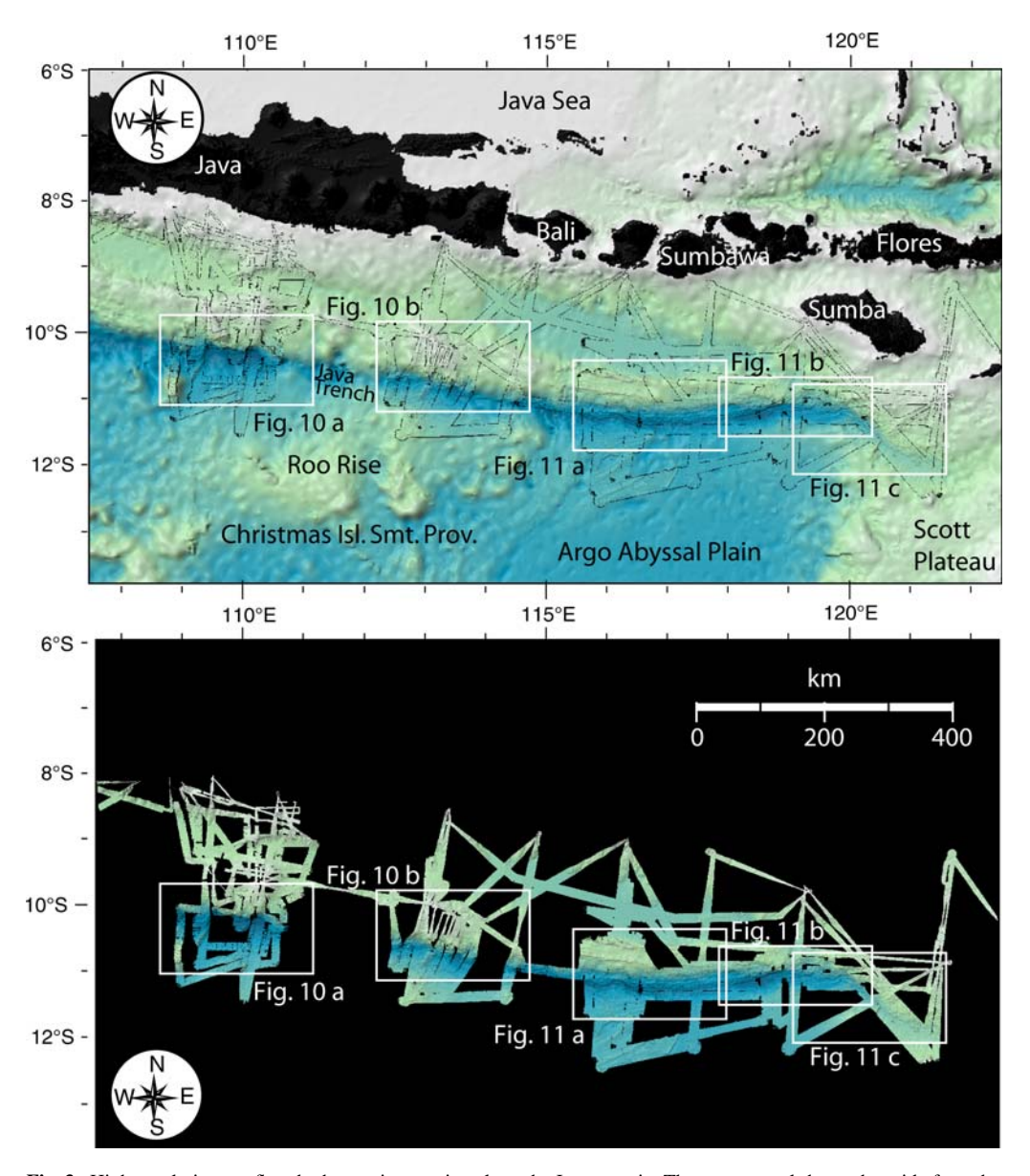


Fig. 3. High-resolution sea floor bathymetric mapping along the Java margin. The upper panel shows the grid of swath data underlain by global bathymetry; the lower panel displays the high resolution data coverage. Full coverage was achieved along the deformation front and lower trench offshore Lombok, Sumbawa and Sumba. RV SONNE's EM120 multibeam echosounder system sends successive frequency-coded acoustic signals. Data acquisition is based on successive emission–reception cycles of this signal. The reception is obtained from 191 beams, with the footprint of a single beam of a dimension of 2° by 2°. Achievable swath width on a flat bottom is up to six times the water depth dependent on the character of the sea floor.

The Java margin exhibits two prominent features on the incoming Indo-Australian plate: (1) the Christmas Island Seamount Province including the Roo Rise and (2) the Argo Abyssal Plain (Fig. 1). The Christmas Island Seamount Province forms a

broad, irregular topographic swell of 135–140 Ma old oceanic lithosphere off central Java (Moore *et al.* 1980; Mueller *et al.* 1997) and is dotted with numerous seamounts. It extends in an east–west direction from 95°E to 115°E, where it terminates

abruptly. The evolution of the Christmas Island Seamount Province remains enigmatic and is associated with a series of individual magmatic events. Rock sampling resolved varying formation times across the volcanic province without a clear formation time trend (Werner et al. 2009). The eastern segment of the Christmas Island Seamount Province features the oceanic Roo Rise (Fig. 1), a 400 km wide plateau rising 2-3 km above the abyssal plain. Dredged rock samples from the plateau retrieved strongly altered olivine phyric lava fragments with Mn-crusts (Werner et al. 2009). The northern flank of the Roo Rise is currently entering the trench south of eastern Java. Isolated volcanic summits on the plateau and adjacent to it represent high relief gradient features which upon subduction cause frontal erosion of the fore-arc south of central Java (Masson et al. 1990). A tomographic study of passive and active seismic data images the complex crustal structure of the fore-arc, segmented into distinct blocks (Wagner et al. 2007).

The second prominent feature in the oceanic domain is the Argo Abyssal Plain, with mean water depth around 5500 m (Fig. 1) and a crustal age of 160 Ma (Mueller et al. 1997). Though large-scale topographic features are not observed on the Argo Abyssal Plain, the sea floor nonetheless exhibits a distinct structure, comprising the original spreading fabric and a pervasive pattern of trench parallel normal faults where the plate bends into the trench (Masson 1991). The horst-and-graben structures on the outer trench wall show a maximum throw of 500 m. Individual fault segments reach lengths of more than 60 km and cut deep into the oceanic basement (Lueschen et al. 2010). 530 m of sediment on the Argo Abyssal Plain have been drilled in DSDP site 261 before reaching Late Jurassic oceanic basement (Heirtzler et al. 1974) on which Cretaceous claystones, Upper Miocene and Pliocene nannofossil oozes and Quaternary radiolarian clays have been deposited. In the east, the Argo Abyssal Plain is bordered by a continental promontory of the Australian lithosphere: the Scott Plateau (Fig. 1) governs subduction zone processes at the transition from the Sunda margin to the Banda arc.

Recent earthquake activity

The Java trench was the site of three major earth-quakes ($\text{Mw} \geq 7.0$) in the past decades (Fig. 1). In 1977, a Mw = 8.3 normal fault earthquake ruptured the underthrusting plate (Spence 1986; Lynnes & Lay 1988) and caused a tsunami on the Lesser Sunda islands and Australia with maximum run-up heights of 8 m on Sumbawa (Kato & Tsuji 1995). The Mw = 7.8 event of 1994 was a megathrust rupture, which occurred offshore eastern Java

(Ammon et al. 2006; Bilek & Engdahl 2007). The triggered tsunami reached run-up amplitudes of 5-8 m along the southern coast of Java, causing more than 700 casualties. Similarly, in 2006, a Mw = 7.7 megathrust earthquake offshore western Java (Fig. 1) triggered a deadly tsunami with maximum run-up heights of 20 m (Fritz et al. 2007). Both thrust events show a rupture pattern characteristic of tsunami earthquakes (Kanamori 1972; Bilek & Engdahl 2007) and both events display aftershock sequences dominated by normal faulting, suggesting relatively complete stress release on the interplate thrust (Ammon et al. 2006). The influence of the plate structure at depth, particularly regarding subducted basement features, has been discussed for the 1994 event, for which slip over a subducted seamount was proposed to have triggered the earthquake (Abercrombie et al. 2001). This model is still debated for the 2006 event (Bilek & Engdahl 2007).

Geophysical data

Three major marine experiments were conducted on the Java margin since 1997 using the German RV SONNE as platform. A total of 289 ocean bottom stations [hydrophones and seismometers: OBH/S (Bialas & Flueh 1999)] were deployed along 13 transects. In 1997/1998, the GINCO cruises focused on the transition zone between frontal and oblique subduction off the Sunda Strait and acquired three coincident seismic refraction/reflection profiles offshore western Java (P05. P06, P07) (Kopp et al. 2001; Schlueter et al. 2002). It was followed by the MERAMEX cruises off central Java in 2004 during which two long refraction dip lines (P16 and P18) were shot from the oceanic lithosphere to the continental slope in addition to a coast-parallel strike-line (P19) (Fig. 1). During this onshore-offshore or amphibious project, 100 landstations were deployed onshore Java for a period of 120 days (Koulakov et al. 2007; Wagner et al. 2007). The eastern section of the margin was subsequently investigated during the SINDBAD experiment in 2006 and was covered by four coincident refraction/reflection dip lines (P42, P31, P22 and P11) and three strike lines (P41, P33, P21) located between offshore eastern Java and east of Sumba island, including the transition from oceanic subduction to continent-island arc collision.

Figure 2 displays the velocity-depth models of all acquired trench perpendicular refraction dip lines and serves as a basis for the following discussion of individual margin segments. All models were achieved by tomographic inversion of the refraction data (Shulgin *et al.* 2009, 2010; Planert

et al. 2010; Wittwer 2010), except for the GINCO profile for which forward modelling by raytracing for the broadly spaced instruments was conducted (Kopp et al. 2001). Figure 4 shows an ocean bottom seismometer recording displaying typical phases from stations near trench locations on the upper plate: Pn is the refraction through the upper mantle, PmP is the reflection from the crustmantle boundary, Poc is the refraction through the oceanic crust, PtocP is the reflection from the top of the oceanic crust and Psed denotes sediment phases. Pg fore-arc is the refraction through the fore-arc crust. The information contained in the seismic record sections thus returns velocity data for the different margin units from the sedimentary cover to the upper mantle.

The bathymetry data (Fig. 3) were acquired during the MERAMEX and SINDBAD experiments using RV SONNE's Simrad multibeam echosounder system, which provides accurate depth measurements and bathymetric mapping in areas at depths down to 11 000 m.

Offshore Sunda Strait and western Java: sediment accretion

Observations

Along the western margin segment (longitudes 105 to 110° E), the incoming oceanic crust is 7.5-8.5 km thick with velocities typical of mature oceanic crust, increasing from 4.7 km/s at the basement to 7.2 km/s at the crust–mantle boundary. Upper mantle velocities are in the order of 7.8-8.0 km/s as documented by Pn mantle phases recorded by the ocean bottom seismometers (e.g. station OBS 42 on line P18 in Fig. 5).

The morphology of the offshore fore-arc of western Java is dominated by a massive fore-arc high above the underthrusting plate (Fig. 2, panels a, b). The tectonic features observed here include the sediment-filled deep-sea trench, an actively accreting prism and mature fore-arc basin. They are morphological manifestations of the accretionary regime continuous to offshore Sumatra (Kopp *et al.*)

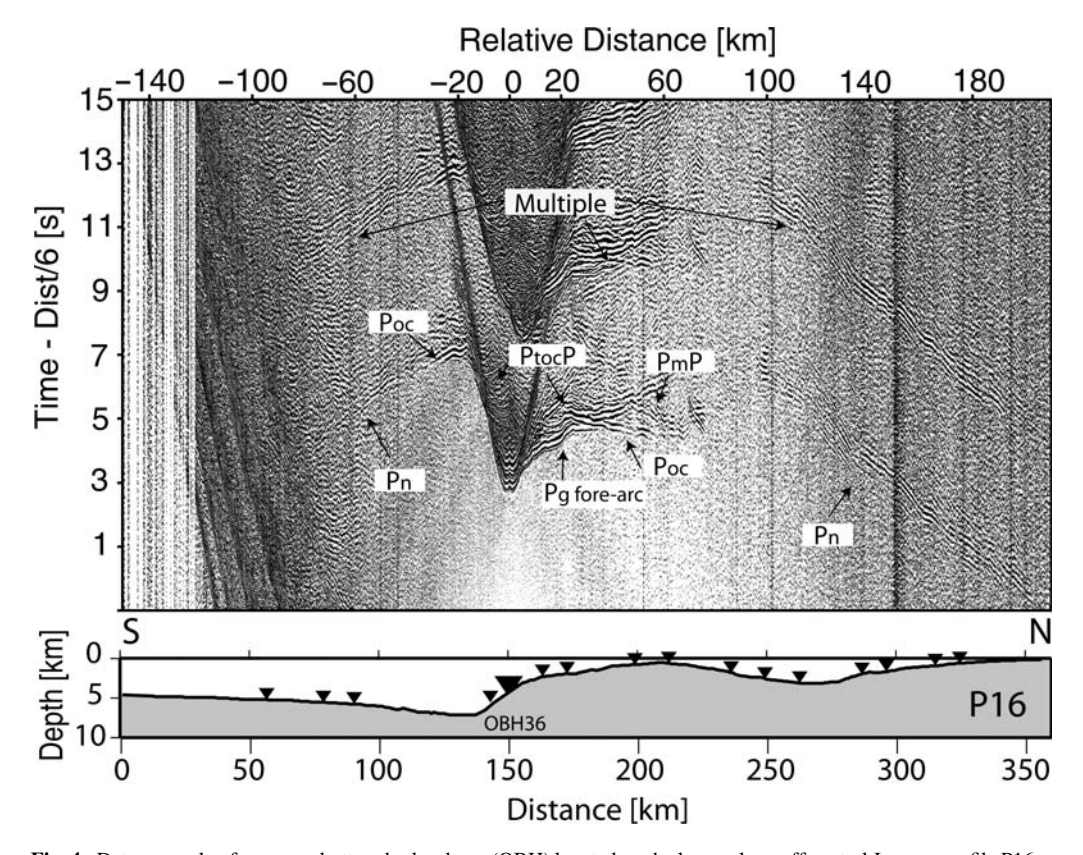


Fig. 4. Data example of an ocean bottom hydrophone (OBH) located on the lower slope off central Java on profile P16. Phase nomenclature is as follows: Pg refraction through fore-arc crust, Poc refraction through oceanic crust, Pn refraction through upper mantle, PtocP reflection from oceanic basement, PmP Moho reflection.

2008), where the fore-arc high is subaerially exposed on the fore-arc islands. Offshore Sunda Strait, the topographic expression of the fore-arc high is subdued as a result of the Neogene transtensional tectonics and the increasing trench-parallel slip component towards Sumatra (Huchon & Le Pichon 1984; Malod *et al.* 1995). Malod & Kemal (1996) estimated about 50–70 km of extension in the Sunda Strait during the Pliocene (Diament *et al.* 1992).

The internal architecture of the fore-arc is characterized by multiple kinematic boundaries between the trench and Java continental slope. The deformation front marks the transition from the trench to the frontal prism which then transitions into the Neogene accretionary prism, that rapidly increases in thickness. In Figure 6, an c. 0.5 km thick sheet of trench sediment is underthrust below the frontal prism. A similar decollement zone is also observed on profile P05 (Kopp et al. 2009), though discontinuous due to subducted seamounts of 1-2 km height attached to the oceanic crust (Fig. 7). This distinct lower plate relief, which is ubiquitous along the Java margin (Masson et al. 1990), potentially breaches the subduction channel and is in contact with the upper plate.

A pronounced megasplay or backstop thrust separates the Neogene prism from the Palaeogene prism (Figs 6 & 7). Seismic velocities increase from the Neogene prism to the older, more consolidated material of the Palaeogene prism. Station OBH 47 on profile P18 (Fig. 8) documents this increase in seismic velocities in the Pfp and Pg phases. The Palaeogene prism is covered by a slope apron with seismic velocities not exceeding 2.5 km/s (Fig. 2, panels a, b). This unit displays little permanent deformation. During the GINCO cruise, Pliocene to recent sediments were sampled at various locations in the fore-arc basin and on the fore-arc high (Beiersdorf 1999). Samples retrieved hemipelagic muds with intercalated turbidites and dacitic to rhyolithic ash layers. Dredge samples from outcrops of the accretionary prism revealed that they consist of silty and micaceous mud and tectonized mudstone as well as of arenitic limestone and calcareous sandstone (Beiersdorf 1999). Unfortunately, rock dredge or drill samples have not been recovered from the core of the fore-arc high, so that its composition must be inferred from seismic velocities.

Offshore western Java, the Palaeogene prism fronts the Java fore-arc basin (Fig. 7). The Java basin is expressed as an elongated, 500 km long subsiding belt with an average water depth of 3500 m. Sediment thickness of the basin infill reaches 4 km (line GINCO p05, Fig. 2), decreasing towards the basin fringe (line Meramex P18, Fig. 2). The basin is underlain by a unit characterized by seismic

velocities rapidly increasing from 5.5 km/s to values larger than 6 km/s (Fig. 2). OBH 53 is situated on the northern rim of the fore-arc high on line P18 and records phases through the Palaeogene prism as well as through the fore-arc crust and mantle (Fig. 9). A number of stations record the fore-arc basement, which shows an ophiolitic character. The basement is exposed in western Java. where outcrops of peridotites, gabbros, pillow basalts and serpentinites are observed (Sukamto 1975; Schiller et al. 1991; Susilohadi et al. 2005). This Cretaceous-Paleocene complex is imaged underneath the fore-arc basin as a seaward dipping unit with the crust-mantle boundary located at c. 15 km depth (Figs 2 (panels a, b & 7). It is bounded to the NW by the Cimandiri fault zone, which cuts the Java fore-arc basin at a direction N70.8°E (Susilohadi et al. 2005) and is traced onshore along the Cimandiri river near Pelabuhan Ratu (Dardji et al. 1994).

Interpretations

At the deformation front, trench sediments are offscraped from the oceanic basement and transferred to the upper plate (Figs 6 & 7). The change from tensional to compressional stress within the trench initiates thrust faulting and accretion of material to the lower slope. Discrete frontally accreted imbricate thrust slices and compressional folding are characteristic of this margin segment (Kopp et al. 2009) (Figs 6 & 7). The imbricate thrust belt and detachment folds form the frontal prism sandwiched between the trench and the Neogene accretionary prism (Kopp et al. 2001, 2002). The frontal prism forms the apex of the upper plate wedge and consists of frontally accreted, fluid-rich and thus mechanically weak material (von Huene et al. 2009). It is within the frontal prism that tectonic addition of trench sediment fill occurs by uplift displacement along the frontal thrust above the decollement (Figs 6 & 7).

The imbricate thrust zone of the Neogene prism is primarily composed of trench sediment transferred from the frontal prism (Figs 6 & 7). The outer Neogene prism pronouncedly contrasts in style from the inner, less compressive Palaeogene prism (Kopp et al. 2001, 2002; Schlueter et al. 2002) (Fig. 7). This contrast in style has been related to the seismogenic behaviour of the subduction fault at depth (Wang & Hu 2006), predicting that the inner wedge never experiences compressive failure, thus providing a stable tectonic regime. The transition from the active Neogene prism to the tectonically more quiescent Palaeogene prism occurs along a distinct zone, where a splay fault system offsets the sea floor (Kopp et al. 2009) (Figs 6 & 7). The surface trace of this thrust fault system is

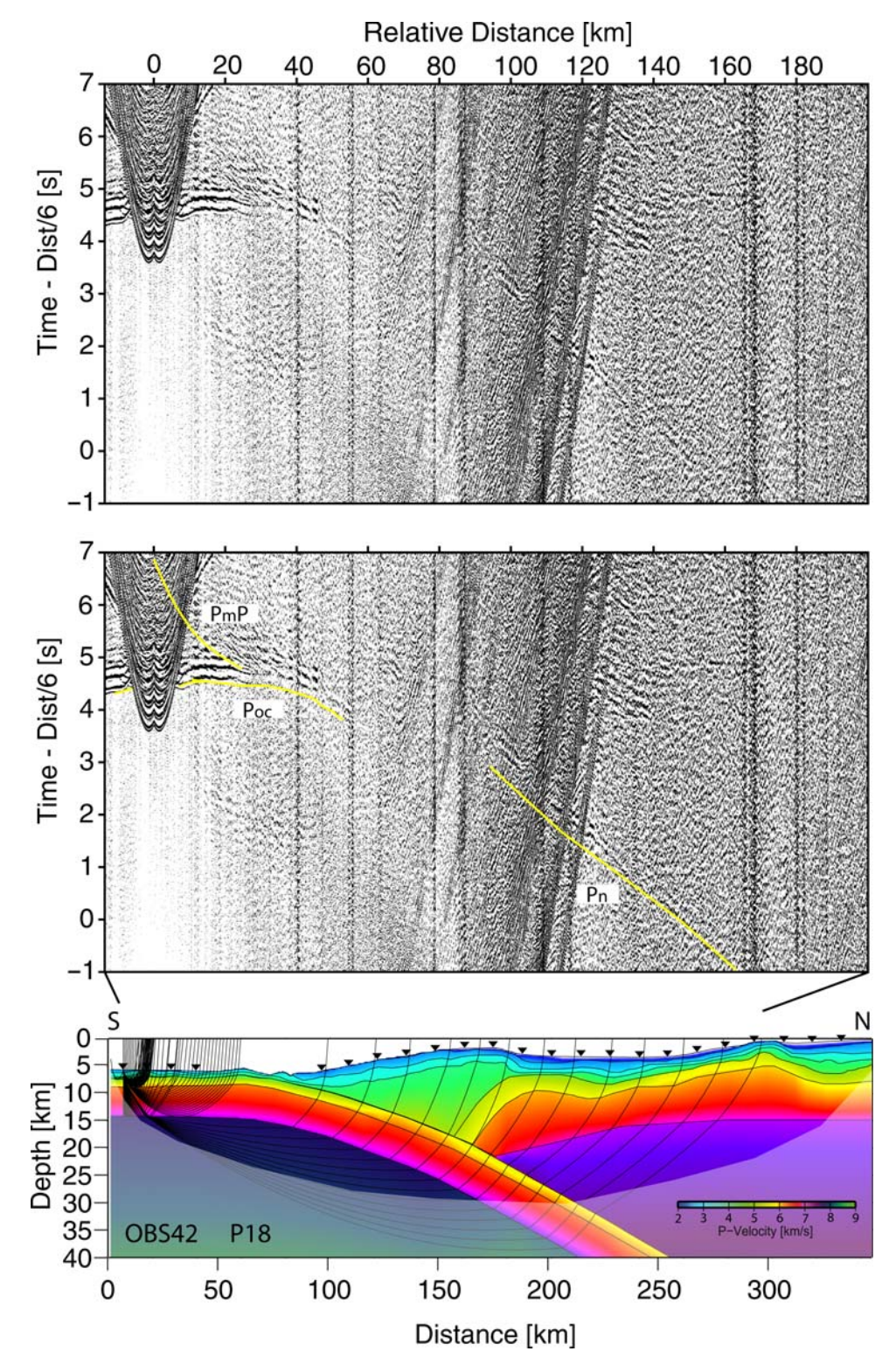


Fig. 5.

observed over a distance of c. 600 km along strike of the margin (Kopp & Kukowski 2003) and implies a continuous segmentation at an average distance of 30-35 km from the deformation front. This transition is also related to a change in surface slope. which decreases from the outer to the inner prism (Figs 6 & 7). The Palaeogene prism, which forms the fore-arc high, serves as backstop to the material accreted in the Neogene prism. Both prisms show active deformation, however, to a much lower degree in the Palaeogene prism compared to its Neogene analogue. The Palaeogene prism forms the core of the large bivergent wedge, which shapes the fore-arc high along the central Sunda margin (Kopp & Kukowski 2003) (Fig. 2, panels a, b). The Late Palaeogene rising of the Himalayan orogenic zone, which is the source for the majority of sediment in the Sumatran and western Java sector of the Sunda trench (Susilohadi et al. 2005), contributed to the evolution of the accretionary fore-arc high, which is directly related to the sediment supply from the Himalayas.

Remaining issues

The internal structure of the Palaeogene prism is not imaged well in reflection seismic data owing to limited energy penetration (Figs 6 & 7). This is a common phenomenon in many accretionary margins and may possibly be associated with internal deformation related to strong shear stress along the underlying seismogenic portion of the subduction fault. In the absence of deep drilling data, information on the composition is primarily gained from wide-angle seismic surveys. Seismic velocities increase from the frontal prism to the Neogene and Palaeogene prisms due to the greater rigidity of the consolidated and lithified material (Fig. 2, panels a, b). Mass balance calculations imply that the Palaeogene prism formed by accretion since the Eocene-Oligocene (Kopp & Kukowski 2003). The deformational segmentation as manifested in the kinematic discontinuities imaged by the refraction data suggests that accretion is non-linear. The rapid landward increase of the wedge thickness accompanied by backthrusting and uplift of the fore-arc high (Fig. 7) are indicative

of basal accretion of the underthrust sequences (Gutscher et al. 1998), however, this process is not unambiguously imaged by seismic methods. Backthrusting along reverse faults is observed on the northern flank of the fore-arc high and initiates a successive northward thrust over the southern portion of the fore-arc basin (Fig. 7) (Schlueter et al. 2002; Susilohadi et al. 2005). The evolution of the Java basin is governed by the accretiondriven uplift of the fore-arc high, which forms a barrier to the trench and abyssal plain and by tectonically induced subsidence forming a rapidly filled depression (Susilohadi et al. 2005). The mechanisms for subsidence remain unclear. In the Sunda Strait, subsidence is likely to be linked to graben formation related to the transtensional regime here (Lelgemann et al. 2000) and the loading effect of Krakatau volcanoclastics (Susilohadi et al. 2005). In western Java, the Ciletuh-Jampang block (Fig. 1) is tilted to the SW. Its subsidence could reflect basal subduction erosion, however, our seismic data fail to image this process. Based on the interpretation of 20 reflection seismic profiles, Susilohadi et al. (2005) tentatively interpreted the oldest sequences in the Java basin to be of Middle Eocene to Late Oligocene age. A regional Upper Oligocene unconformity is traced as an erosional surface in the fore-arc basins from northern Sumatra to central Java (Fig. 7) and indicates that prior to the Neogene the shelf area was dominated by subaerial exposure or shallow water conditions (Susilohadi et al. 2005). This is also supported by well data from the shelf and onshore outcrops (Susilohadi et al. 2005). Later, sediment supply increased during the late Middle Miocene with the rising volcanic activity of the arc (Susilohadi et al. 2005).

Offshore central-eastern Java: seamount subduction and fore-arc erosion

Observations

The central-eastern Java segment is characterized by the subduction of an oceanic plateau, the Roo Rise, which is dotted with abundant basement

Fig. 5. Seismic wide-angle section for ocean bottom seismometer OBS 42 of line P18 (upper panel), where 23 instruments were deployed (black triangles in lower panel). The gap in instrument spacing in the trench is due to the great water depth exceeding the instrument's pressure tolerance. The middle panel illustrates the calculated travel times on top of the seismic data shown in the upper panel. Rays in the lower panel are shot through a forward model with a velocity-depth distribution based on tomographic inversion. Shaded areas are not well resolved. A pronounced *Pn* mantle phase is recorded through the oceanic upper mantle reaching offsets of 160 km. The bending geometry of the oceanic crust underneath the trench inhibits ray coverage and results in a gap in first arrivals at 60–80 km offset. Consecutive inversion of different phases using a top-to-bottom approach recovered crustal and mantle velocities successively. See Figure 4 caption for phase information.

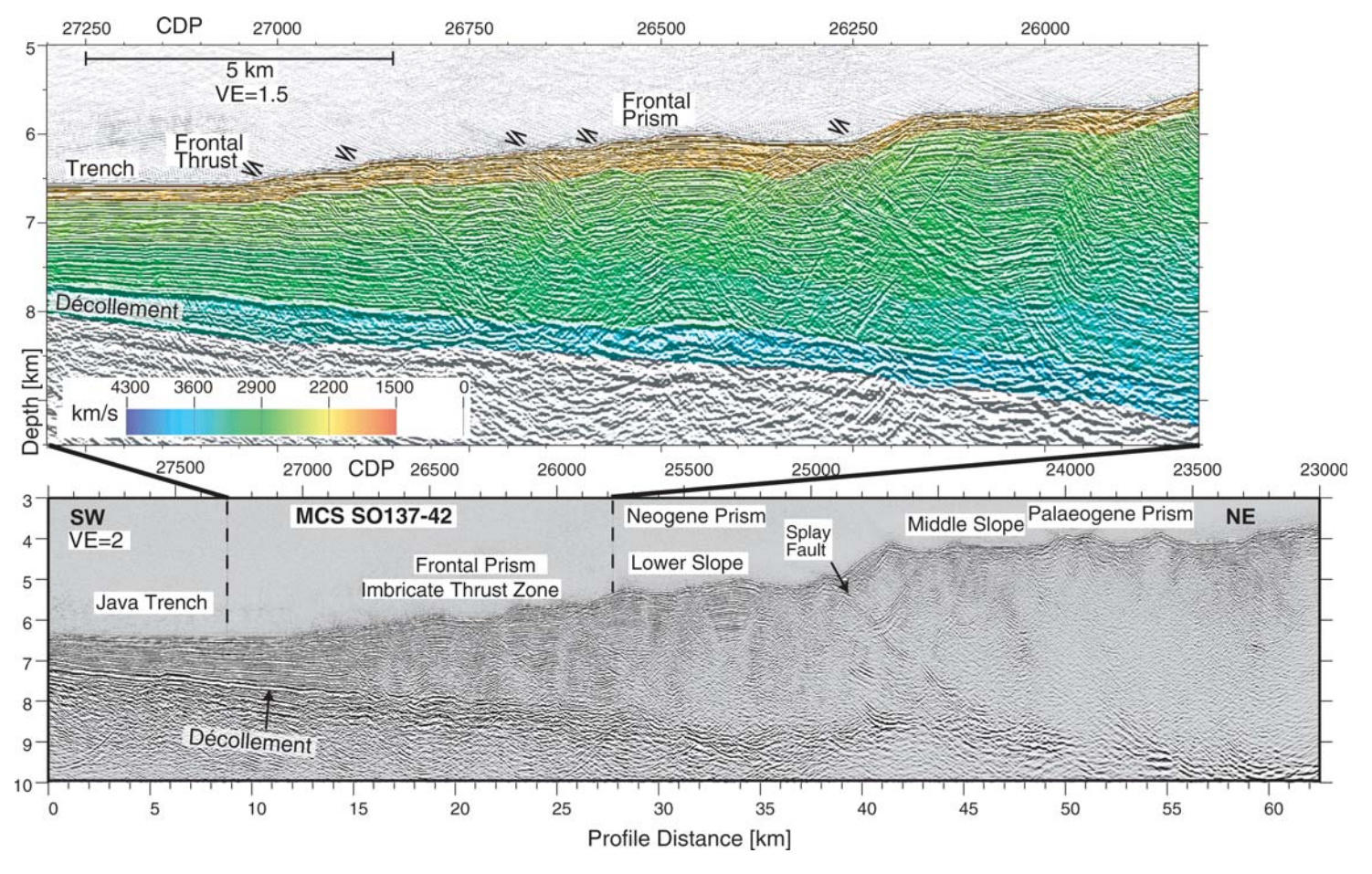


Fig. 6. Pre-stack depth migrated multichannel seismic data crossing the deformation front and trench offshore Sunda Strait. Location is shown in Figure 1. The lower panel shows the underthrusting of the Indo-Australian crust underneath the lower and middle slopes of the overriding plate. In the upper panel, the fold-and-thrust belt of the frontal prism is imaged with at least four consecutive pairs of forethrusts and backthrusts. Trench sediment is uplifted along the frontal thrust and subsequently rotated as it is incorporated into the frontal prism. The lowermost 400–500 m thick unit of trench fill is underthrust beneath the frontal prism. A splay fault marks the transition from the Neogene accretionary prism to the Palaeogene prism and coincides with a change in slope angle. Seismic velocities are interval velocities obtained during pre-stack depth migration. The MCS data were acquired by the BGR, Hannover, during the GINCO cruise.

relief (Masson *et al.* 1990). Relief elevation above the surrounding sea floor ranges from hundreds of metres to over 2 km. Oceanic crustal thickness is increased where the crust is altered by the emplacement of the Roo Rise. Profile P16 (Fig. 1) documents a crustal thickness of 9 km on the flank of the Roo Rise seaward of the trench (Fig. 2, panel c). Line P42, located off eastern Java and covering the Roo Rise south of the trench (Fig. 1), shows a pronounced Moho topography, with crustal thickness decreasing from 18 km in the oceanic domain to 11 km underneath the trench (Fig. 2, panel d).

The high-resolution bathymetry maps the underthrusting of basement relief underneath the upper plate, for example the incipient subduction of a small ridge (Fig. 10b) currently positioned in the trench. Larger topographic features on the oceanic plate are resolved by the global bathymetry (e.g. a moderate-sized seamount of 70 km diametre at a distance of 40 km from the trench (Fig. 10a)). The surface effect of seamount subduction and the corresponding deformation of the lower slope are revealed well in the absence of a thick sediment apron, as is the case for central Java (Fig. 10). Frontal erosion has sculpted the lower slope off central and eastern Java and is associated with a northward retreat of the deformation front by up to 60 km (Kopp et al. 2006). This segment of the Java margin shows extremely high surface slope values at the lower slope of the overriding plate, reaching values $> 13^{\circ}$ (Kopp *et al.* 2006).

Sea floor topography based on global satellite altimetry data (Smith & Sandwell 1997) reveals that the fore-arc high is characterized by isolated topographic summits between 109-115°E trending in a NW-SE direction parallel to the trench at roughly 10°S (Kopp et al. 2006) (Fig. 1). They rise to water depth of 750-1000 m and are roughly 1 km higher in elevation than the surrounding fore-arc high. This is documented by the two adjacent seismic profiles P16 and P18 (Fig. 2, panels b, c). The western line is located in the accretionary domain as described above and crosses the easternmost portion of the Java fore-arc basin. The eastern profile is positioned on the flank of the Roo Rise (Fig. 1). The difference in elevation of the fore-arc high on these two lines is c. 1000 m (Fig. 2, panels b, c). Further landward, a broad swell located between profiles P18 and P42 (Fig. 1) is anomalous along the Sunda Arc's coastlines.

The tomographic inversion of profile P16 (Fig. 2, panel c) images a strongly deformed fore-arc and basin, which extends for 50 km in a north-south direction (compared to 80 km on line P18 (Fig. 2, panel b)). Approximately 4 km of volcanic ashes and sediment are trapped in the basin, which is carried by the landward tilted basement above the Java unconformity (Fig. 11). At a depth of

c. 14 km, the inversion images a subducted seamount around profile km 190 (Fig. 2, white arrow in panel c). The accretionary prism offshore Java is characterized by velocities generally not exceeding 5.0 km/s (Fig. 2). The subducted relief is inferred from the higher velocities (vp > 5.4 km/s) at the base of the accretionary prism retrieved along P16. OBH 30 (Fig. 12) covers the entire fore-arc and records the internal structure of the accretionary prism and subducting slab. Imaging, however, is intricate due to the severe deformation in this domain.

Interpretations

The transition from frontal accretion along the western Java segment to frontal erosion off central Java occurs over a short distance of some tens of kilometres and is documented by the two adjacent seismic profiles P16 and P18 (Fig. 2, panels b, c). The central Java margin segment is currently experiencing frontal erosion associated with the underthrusting of the Roo Rise. The northward migration of the Java Trench and deformation front above the leading edge of the Roo Rise has exposed an area of c. 25 000 km² of deeper sea floor formerly covered by the upper plate (Kopp et al. 2006). The corresponding northward shift of the axial position of the trench by about 60 km is moderate and may reflect a relatively recent onset of plateau subduction coupled with the arrival of the Roo Rise and Christmas Island Seamount Province at the trench. Based on the global satellitederived bathymetry (Fig. 1), Shulgin et al. 2010 infer that the edge of the plateau, which already subducted, could be located as far as 70 km north of the trench, which would correspond to an onset of plateau subduction at 1.1-1.3 Ma ago. However, there is no direct evidence.

Topographic basement relief is abundant on the lower plate offshore Java (Masson et al. 1990) and modulates the structure and morphology of the overriding plate at various scales. The morphological perturbations of the lower slope resulting from subduction of oceanic relief depend on the size and structure of the subducted feature and on the nature of the overriding plate. Seamount subduction has been investigated at erosive margins (e.g. von Huene et al. 2000) where the seamounts leave pronounced re-entrant grooves as they plough through the small frontal prism before being subducted beneath the continental framework rock (von Huene 2008). Comparable embayments are not as distinct offshore Java (Fig. 10), where the accretionary material behaves more plastically. Topographic perturbations resulting from seamount subduction within the frontal prism are transient and the prism will heal after the relief is

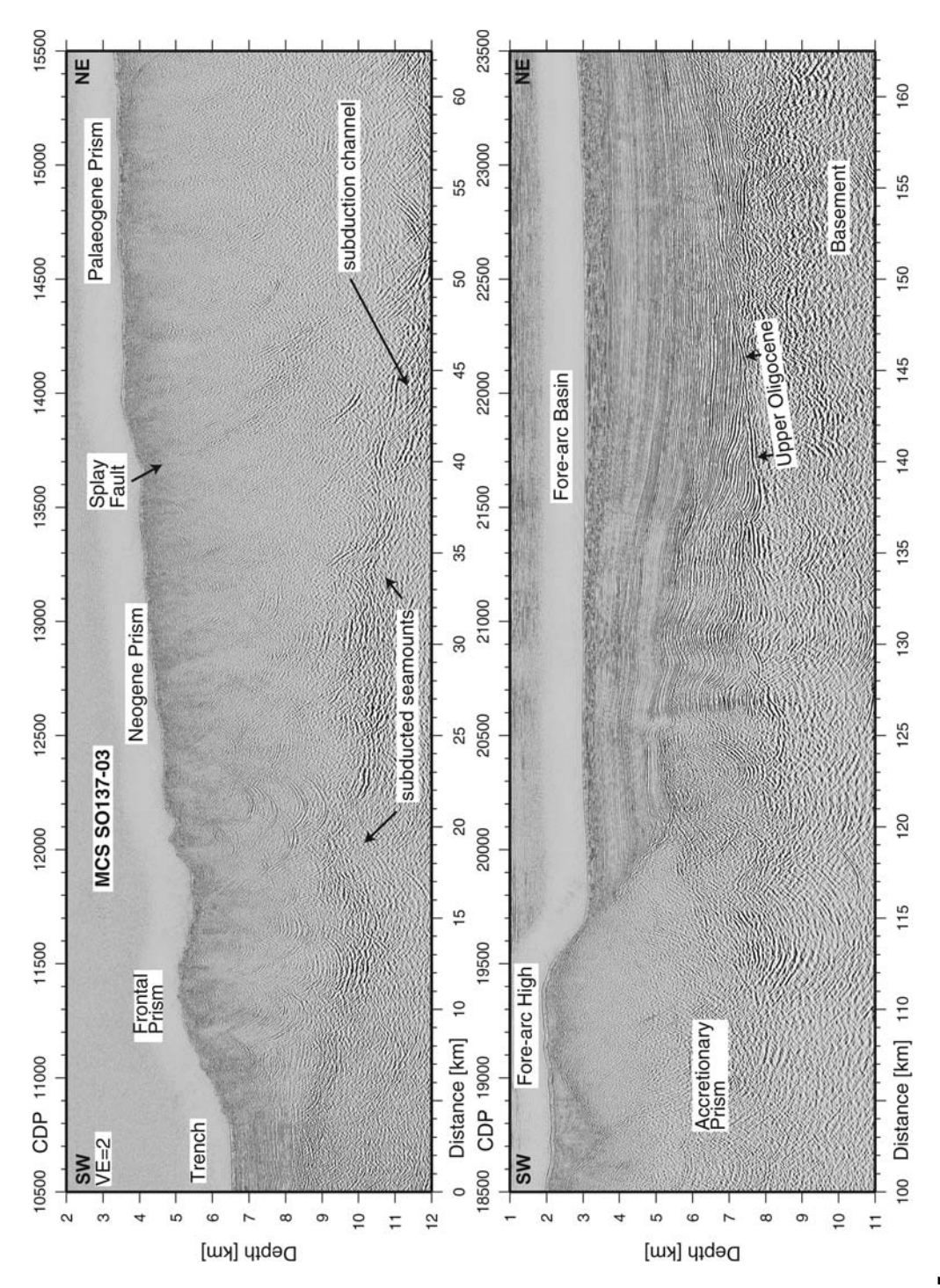


Fig. 7.

subducted to greater depth. Frontal erosion coincides with a steepening of the lower slope angle in the central Java sector compared to the neighbouring segments (Kopp *et al.* 2006), bringing the taper into the unstable domain here. This results from subduction of basement relief, which at first causes deformation and uplift of the thin leading edge of the fore-arc (Taylor *et al.* 2005). The unstable frontal prism is marked by small-scale re-entrant scars (Fig. 10), by mass failure and extensional normal faulting (Fig. 10a). Erosive processes are enhanced by the lack of sediment in the trench and the pronounced horst-and-graben structure in the trench where the plate bends underneath the fore-arc (Fig. 10b).

Tectonic modification of the fore-arc offshore central to eastern Java is expressed in regional uplift affecting the entire marine fore-arc as well as in isolated zones of increased elevation (Fig. 1). The regional uplift pattern is caused by the subduction of the buoyant oceanic plateau, which results in uplift of the shelf as also described for the Hikurangi margin offshore New Zealand (Litchfield et al. 2007). Although due to the lack of independent data the onset of plateau subduction cannot be verified, it seems likely that it has been occurring since the late Pliocene when uplift and deformation of the upper plate intensified (Shulgin et al. 2010). Crustal thickening occurs mainly in the lower crust and seismic as well as gravity data confirm the presence of a crustal root here (Shulgin et al. 2010) as postulated by Newcomb & McCann (1987) to explain the absence of a correlated gravity anomaly. These results confirm numerical models, which predict crustal thickening to be concentrated in the gabbroic/basaltic layers (van Hunen et al. 2002). The observed thinning of the oceanic crust on profile P42 (Fig. 2, panel d) may either represent a local volume variation or may image the northern rim of the igneous expression. Subduction of smaller scale high relief gradient features likely accounts for the short wavelength anomalies observed along the fore-arc high (Masson et al. 1990; Abercrombie et al. 2001; Kopp et al. 2006). The observed uplift on profiles P18 and P42 (Fig. 2) panels c, d) is inferred to be caused by the impingement of oceanic basement relief and the associated

deformation. A trench perpendicular compressive force is applied on the fore-arc by the relatively buoyant and thick subducting Roo Rise and its volcanic summits. This effect has also been reported for other margins, for example the Ryukuyu margin (Font & Lallemand 2009), Hikurangi margin (Litchfield et al. 2007), Costa Rica margin (Fisher et al. 2004) or the New Hebrides/Solomon arcs (Taylor et al. 2005). Uplift results from isostatic adjustment and is enhanced by crustal shortening of the overriding plate. The trench perpendicular compression leads to surface elevation of the forearc high, which greatly exceeds the original height of the seamount, as predicted by numerical modelling (Gerya et al. 2009). Surface uplift of 1 km is observed on P16 (Fig. 2, black arrow in panel c) and correlates with the position of the seamount at depth. Uplift is generated by crustal shortening and thickening of the overriding plate over a locked segment of the subduction thrust (Taylor et al. 2005). Backthrusting of the fore-arc high onto the fore-arc basin (Fig. 7) is observed along the entire segment and partially accommodates fore-arc convergence (e.g. Taylor et al. 1995).

In addition to the deformation of the overriding plate, a subducted seamount at depth experiences faulting and possible rupture. Baba et al. (2001) investigate the stress field associated with seamount subduction and conclude that shear failure and fracturing or dismemberment of subducting seamounts occur. This will in turn affect seismic velocities and limit the velocity contrast between the accretionary prism and the subducted seamount. Regarding the subducted seamount detected on line P16, gaps in the ray coverage along the profile certainly inhibit the imaging (Fig. 2, panel c). The presence of a seamount is, however, supported by a number of very distinct surface effects that document the dynamic influence of seamount subduction on the fore-arc morphology. These effects are associated with the subduction of moderate-sized features (Dominguez et al. 2000; Gerya et al. 2009) and include local surface uplift, topographic perturbation of the lower slope, intensification of subduction erosion, and landward trench displacement. All of these key indicators are recognized off central Java (Fig. 2, panels c, d) (Kopp et al. 2006).

Fig. 7. Pre-stack depth migrated multichannel seismic data offshore western Java. Location is shown in Figure 1. The upper panel shows the southwestern extent of the profile from the trench to the Palaeogene prism, the lower panel displays the landward part of the line from the fore-arc high to the fore-arc basin. In the frontal prism, shortening is accommodated by imbricate thrusting of the frontally accreted sediment. Approximately 1/3 of the trench material is underthrust beneath the frontal prism in a 500-900 m thick decollement zone, characterized by discontinuous high amplitudes. Two subducted oceanic basement highs of c. 1.4 and 0.8 km height, respectively, are imaged along the decollement zone. As off Sunda Strait (Fig. 6), a splay fault separates the Neogene and Palaeogene prisms and connects to the megathrust at depth. In the lower panel, sedimentary sequences above an Upper Oligocene unconformity are deformed by thrusting at the seaward part of the basin. The MCS data were acquired by the BGR, Hannover, during the GINCO cruise. After Kopp et al. (2009).

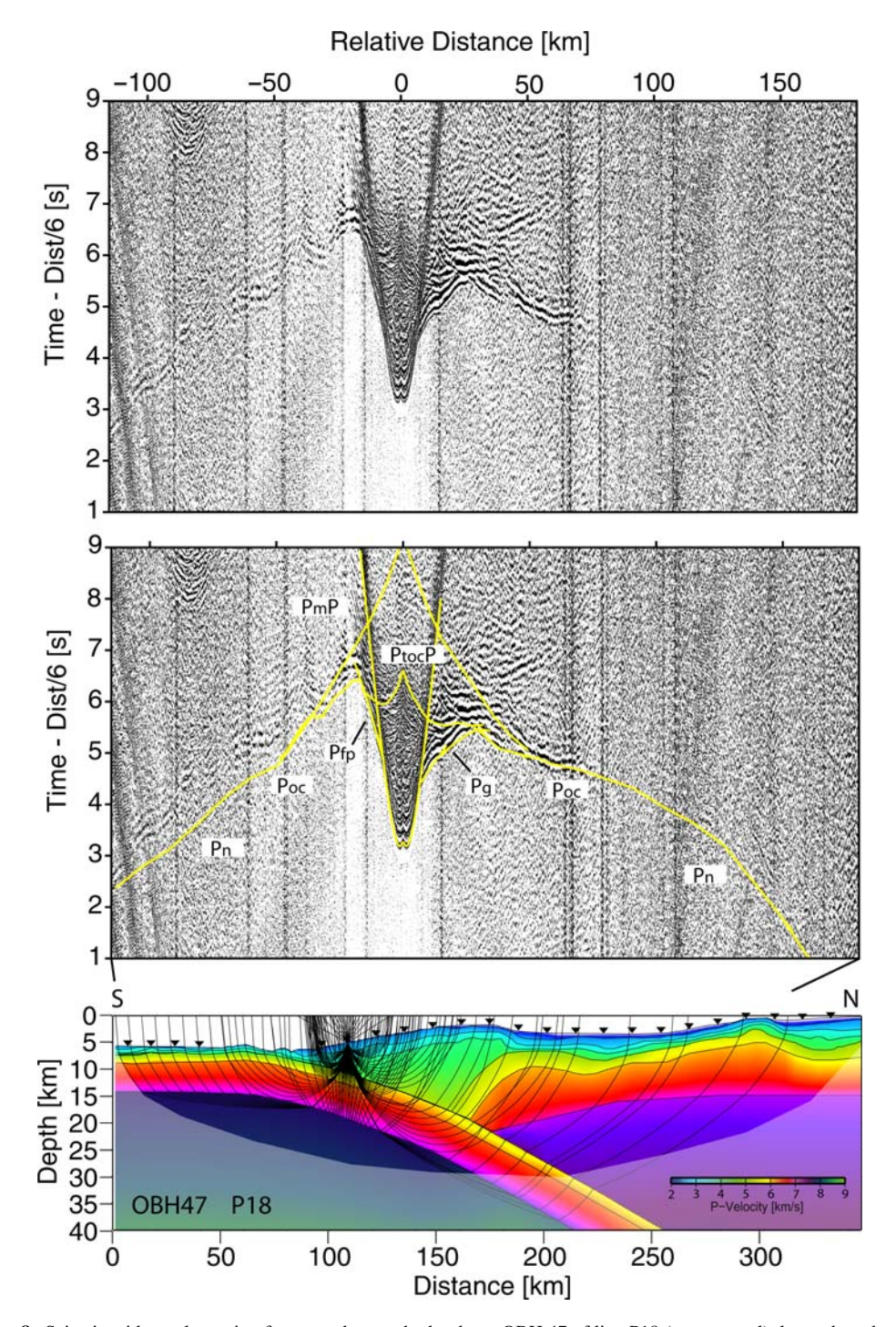


Fig. 8. Seismic wide-angle section for ocean bottom hydrophone OBH 47 of line P18 (upper panel), located on the lower slope off western Java. The middle panel illustrates the calculated travel times on top of the seismic data shown in the upper panel. The landward increasing velocities of the fore-arc are documented by phases Pfp and Pg, which travel through the frontal prism and Neogene/Palaeogene prism, respectively. See Figures 4 and 5 captions for additional phase and display information.

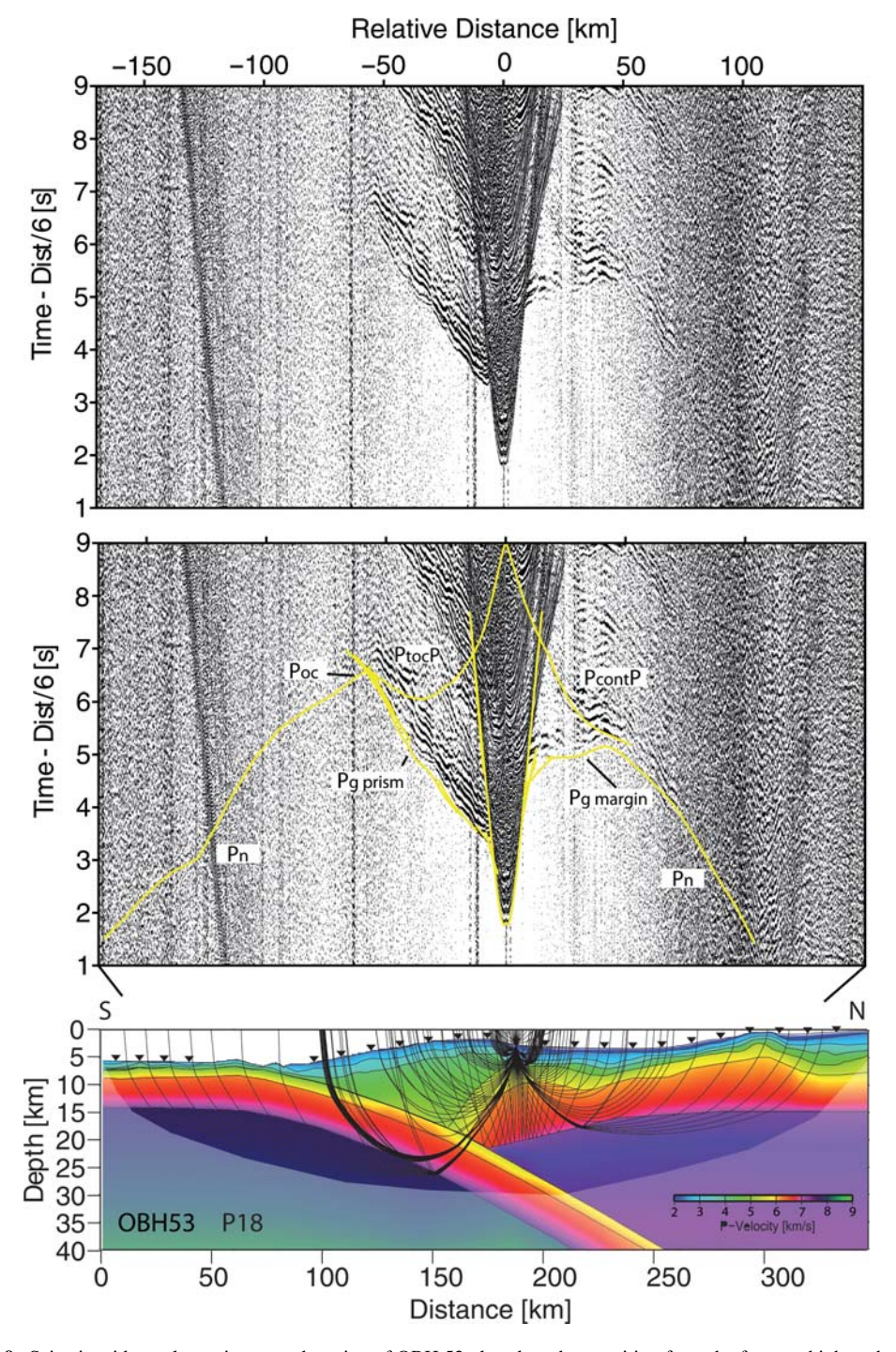


Fig. 9. Seismic wide-angle section record section of OBH 53 placed on the transition from the fore-arc high to the fore-arc basin on line P18 offshore western Java. Record phases through the Palaeogene prism (*Pg prism*) reveal slower velocities here compared to the fore-arc crust (*Pg margin*) and mantle (*Pn*). Strong reflections from the upper plate Moho (*PcontP*) specify the depth to the crust—mantle boundary below the fore-arc basin. See Figures 4 and 5 captions for additional phase and display information.

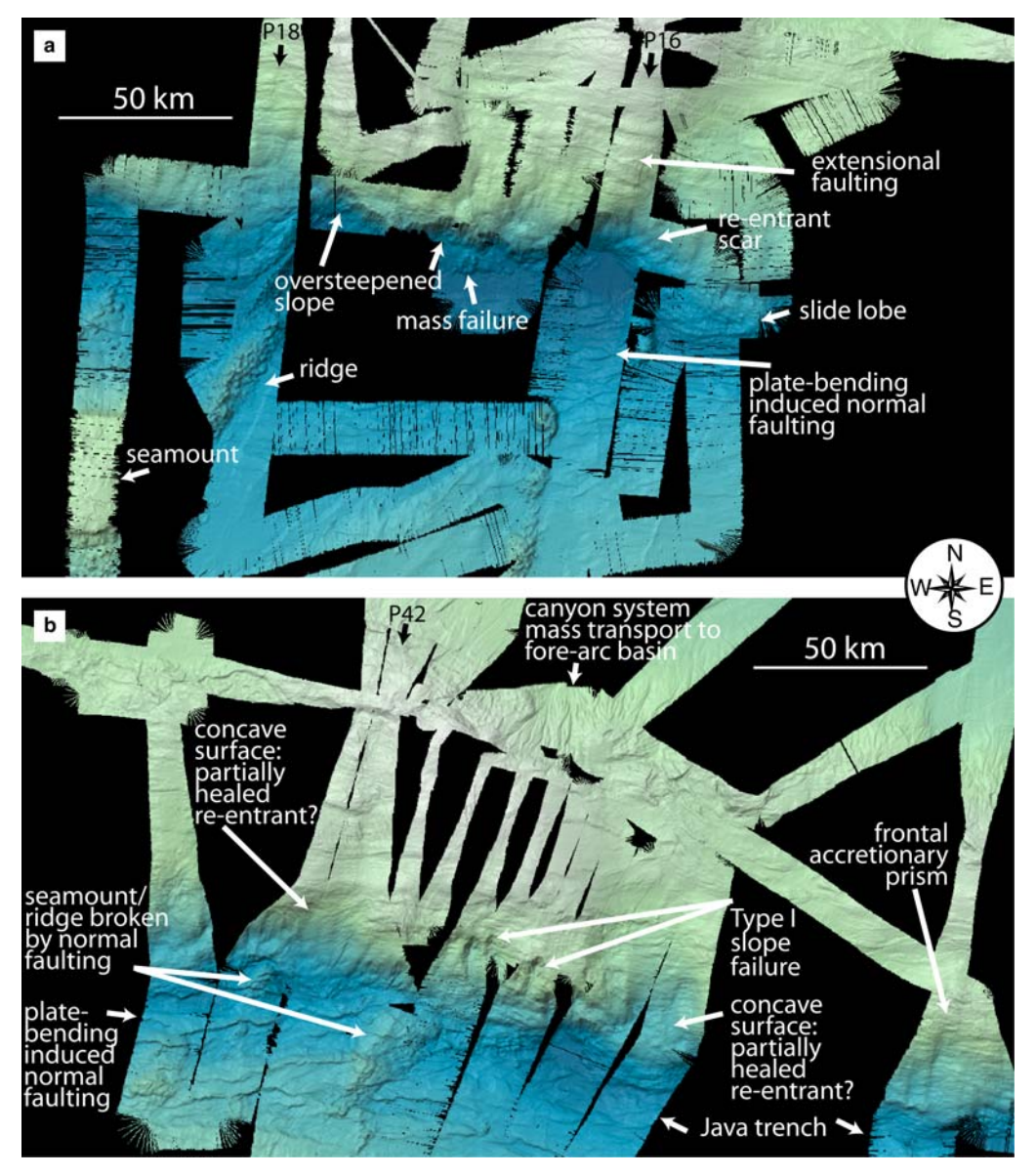


Fig. 10. High-resolution bathymetric mapping offshore central-eastern Java. The swath lines represent the ship tracks, for example, along profiles P16, P18 and P42. Black background is not covered by data. Black pings are data artifacts. Light colours represent shallow water depth, dark blue colours represent deeper water. (a) shows the trench and lower slope offshore central Java. Location is indicated in Figure 3. The lower slope is heavily sculpted by subducting sea floor relief. The oversteepened slope locally fails and mass wasting onto the trench floor occurs. A large, 20 km wide re-entrant scar along the track of profile P16 indicates subducted sea floor relief, resulting in extensional faulting related to uplift. (b) images the trench floor disrupted by plate-bending induced normal faulting, which also affects basement relief. Type I landslides are observed along the lower slope. Two locations exhibit a concave surface slope, indicative of re-entrant scars, which have partially healed. Material is effectively transported from the fore-arc high into the fore-arc basin along extensive canyon systems.

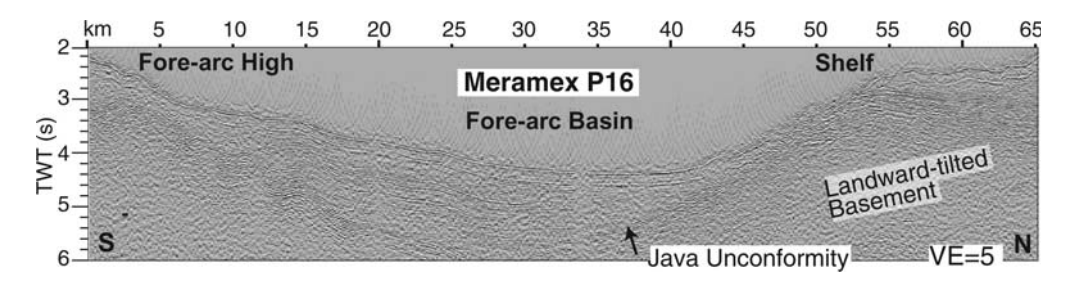


Fig. 11. Four-channel streamer section across the central Java fore-arc basin. Location is shown in Figure 1. The fore-arc basin strata onlap the fore-arc high and are tilted landward, indicating syndepositional and postdepositional vertical movement of the seaward portion of the basin and the fore-arc high.

Remaining issues

Profile P42 crosses the hypocentre location of the 1994 Java Tsunami earthquake (Abercrombie et al. 2001; Polet & Thio 2003; Bilek & Engdahl 2007) (Fig. 1). The reverse mechanism event, which is associated with slip at a previously wellcoupled subducted seamount, showed normal faulting aftershocks that have been related to extension in the outer rise area (Abercrombie et al. 2001). This concept is supported by the high-resolution bathymetry of the trench area, which resolves platebending induced normal faulting (Fig. 10b) with vertical offsets of up to 500 m. The tomographic inversion of P42 as well as a corresponding multichannel line show indications of deeply penetrating faults (Lueschen et al. 2010; Shulgin et al. 2010) affecting the oceanic crust in the vicinity of the trench (Fig. 2, panel d). The deep structure of the fore-arc resolves the intricate geometry of the accretionary complex, which is characterized by heterogeneous uplift and deformation patterns. The velocity-depth distribution (Fig. 2, panel d) suggests the presence of accreted oceanic crustal fragments or detached oceanic basement relief. Remnants of accreted seamounts have been proposed to be present in the Japanese island arc (Isozaki et al. 1990), indicating shearing off and crustal underplating of oceanic basement material (Uchida et al. 2010). This scenario would also explain the fore-arc structure along P42. An anomalous high velocity structure is present at a depth of 13 km (Fig. 2, panel d). It is unlikely that a subducted seamount would still be intact under these conditions. Figure 10b maps the incipient subduction of a small seamount, which currently collides with the deformation front. This seamount as well as other bathymetric features in the trench and on the outer rise is broken by the bending-related normal faulting. The surface traces of the faults are continuous across the sea floor relief. Dismemberment of a seamount or oceanic crustal fragment will decrease seismic velocities and lower the velocity contrast to the surrounding accretionary prism. As a consequence, seismic imaging will be distorted.

Offshore the Lesser Sunda islands: transition from oceanic subduction to continent—island arc collision

Observations

The margin segment south of the Lesser Sunda islands shows a different structure compared to its western counterpart. Here, a mature fore-arc basin, the Lombok basin, is observed at a water depth of 4400 m, which is limited to the west by the uplift associated with the Roo Rise subduction to the east and by collision of the Scott Plateau with the crystalline crust of the Sumba Island (Fig. 1) (Shulgin et al. 2009; Planert et al. 2010). The fore-arc high and accretionary prism are much more uniformly developed than in the neighbouring sector off Java, where isolated bathymetric elevations dominate the fore-arc high topography. Off Bali and Lombok, the fore-arc high is dominated by two elongated tectonic ridges (Fig. 13a) (Mueller et al. 2008; Krabbenhoeft et al. 2010) and diminishes in size and volume to the east.

The age of the oceanic lithosphere decreases from Late Jurassic at 120°E to Early Cretaceous around 110°E (Heine *et al.* 2004; Mueller *et al.* 2008). On the incoming plate, Planert *et al.* (2010) determine a crustal thickness of 8.6 km off Lombok, increasing to 9.0 km to the east near the transition to the Scott Plateau. The transition from the oceanic crust of the Argo Abyssal Plain to the subducting crust of the Scott Plateau occurs over short distances of less than 50 km (Fig. 13c) and concurs with an increase in crustal thickness of *c.* 5 km, mainly accommodated by the upper crust (Fig. 2, panels f, g) (Planert *et al.* 2010).

Convergence occurs at a rate of c. 70 mm/a in a direction N13°E offshore Bali (Simons et al. 2007).

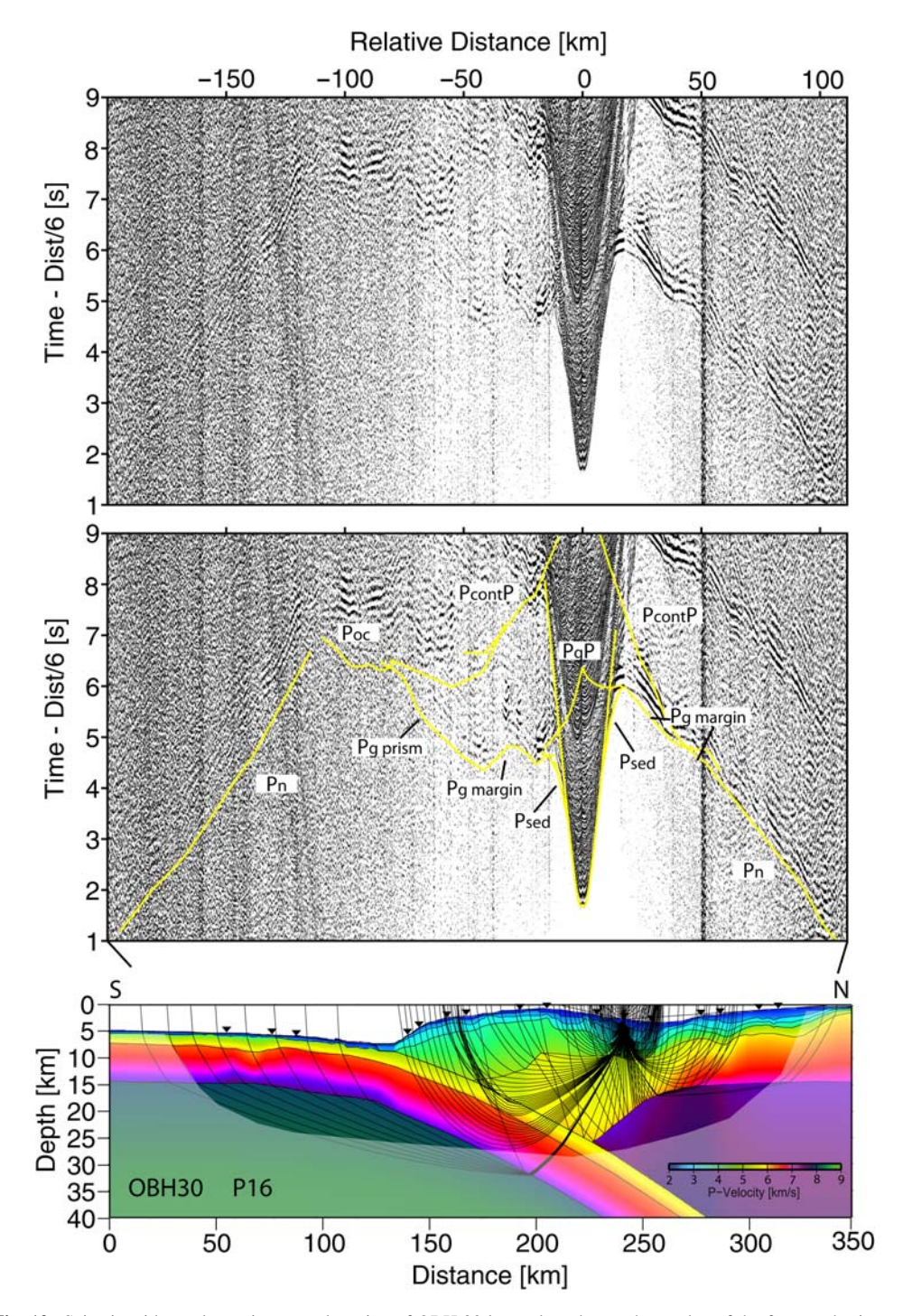


Fig. 12. Seismic wide-angle section record section of OBH 30 located on the southern edge of the fore-arc basin offshore central Java on profile P16. This station covers the entire subduction complex and reveals the velocity structure of the accretionary prism (*Pg prism*) and the deep structure of the fore-arc (*Pg margin* and *PcontP*). *PgP* is the fore-arc crust basement reflection. The oceanic *Pn* phase to the south is reverse to the according phase on station OBS 42 displayed in Figure 5. See Figures 4 and 5 captions for additional phase and display information.

Figure 13 displays oceanic basement structures in the Argo Abyssal Plain trending at angles of 45-60°. Planert et al. (2010) argue that these structures trace the original sea floor spreading fabric as they trend parallel to the magnetic anomalies (Lueschen et al. 2010). Approaching the trench, plate bending induced normal faulting starts to dominate the sea floor fabric within 40 km of the trench axis (Fig. 13) (Planert et al. 2010). The resulting rough topography of the oceanic basement can be traced to several kilometres depth underneath the accretionary prism. Riffling of slope debris subparallel to the underthrust horst-and-graben relief is observed for parts of the frontal prism (Fig. 13a), similar to processes observed in northern Chile (von Huene & Ranero 2003). This region corresponds to reduced upper mantle velocities, which reach values of 7.5 km/s within a distance of 30-50 km from the trench (Fig. 2, panels e, f).

The fore-arc high rises steeply from the trench to water depth of less then 2500 m (Fig. 13a). Localized slope failure is observed on Figure 13 and is associated with the oversteepening of the lower slope. The sea floor morphology is dominated by two distinct, east-west trending ridge structures (Ridge A and Ridge B in Fig. 2, panel e) spaced c. 25 km apart (Fig. 13a). Uplift and tilting of piggyback basins hosted between the ridges (Fig. 13a) document active deformation and vertical displacement (Mueller et al. 2008). Seismic velocities of the fore-arc high do not exceed 5.5 km/s where it is in contact with the underthrusting oceanic crust at a depth of c. 13 km (Fig. 2, panels d, e), indicating a sedimentary composition as inferred for other parts of the margin. This is also supported by the relatively smooth magnetic response of the forearc high (Mueller & Neben 2006). The fore-arc high is fronting the Lombok basin, which carries 3-4 km of sediment above a seaward dipping basement (Fig. 2, panels d, e). The c. 9 km thick basement crust underneath the basin shows a high velocity gradient in its upper portion, decreasing in the lower crust. The upper plate Moho is located at a depth of c. 16 km underneath the fore-arc basin (Fig. 2) with upper mantle velocities of 7.5- $7.6 \,\mathrm{km/s}$.

Interpretations

Sediment recycling is the principal process of mass flux along the lower slope south of the Lesser Sunda islands, where mass wasting of the fore-arc high supplies upper plate material to the trench (Fig. 13b), which is subsequently incorporated into the frontal prism. The oceanic crust is progressively faulted and altered as it approaches the trench. The complex shape of the thrust interface as imaged in the tomographic models (Fig. 2, panels d-g)

suggests a high degree of fracturing of the oceanic crust with potential dissection into singular blocks. Horst-and-graben structures with vertical offsets of up to 500 m are recognized along the outer trench wall (Fig. 13a-c). Where the lower plate relief is not as pronounced, the lower slope is not impacted by subducted seamounts and is characterized by thrust faults (Fig. 13a). Offshore Bali and Lombok. the middle slope largely remains undisturbed, however, local undulations in the topography may result from lower plate fabric subducted beyond the frontal prism. A number of landslides have been identified along this margin sector (Brune et al. 2010a) and are classified into two types (Types I and II) as proposed by Yamada et al. (2010). Type I slides are of smaller dimension, developing on the lower slope and occurring frequently. The frequency of Type II slides is much lower compared to Type I failures. They occur on the middle and upper slope and are of larger dimension compared to Type I slides. Offshore Sumbawa at 117°52′E/ 11°4′S, a Type II slide on the middle and lower slopes at 5300 m water depth with a width of 23 km affected a volume of c. 15 km³ (Brune et al. 2010a) (westernmost slope failure in Fig. 13b). From the absence of a deposition lobe it may be inferred that the landslide sediment deposit has been frontally accreted and incorporated into the frontal prism seaward of the headwall scarp. A northward offset of the headwall scarp indicates segmentation of the slide and collapse in successive events. Moving to the east, at least three adjacent slope failures (Type I) are identified in Figure 13b. They are of much smaller volume and only affect the lower slope. Lateral migration of slope failures has been predicted by analogue modelling (Yamada et al. 2010). The primary single slide will lead to changes in slope topography due to sediment displacement. Adjacent areas then become instable due to the resulting topographic undulations and another event is triggered in adjacent areas. The largest slide (Type II) with a volume of 20 km³ (Brune et al. 2010a) is encountered at $119^{\circ}15'E/$ 11°3′S where it has left a significant deposit lobe resulting from failure of the middle and lower slope (Fig. 13b, c). This is located in the transition area from oceanic subduction to continent-island arc collision at the easternmost end of the Java trench. A sequence of seaward vergent normal faults on the outer trench wall relays the deepening of the sea floor from the Argo Abyssal Plain with a water depth of <5000 m to the trench at 6500 m depth below the sea surface (Fig. 13b) (Planert et al. 2010). Near the deformation front, two landward vergent faults with a strike of c. 65° and thus subparallel to the magnetic anomalies (Mueller et al. 2008) are sculpting the deformation front and lower slope as they are subducted (Fig. 13c).

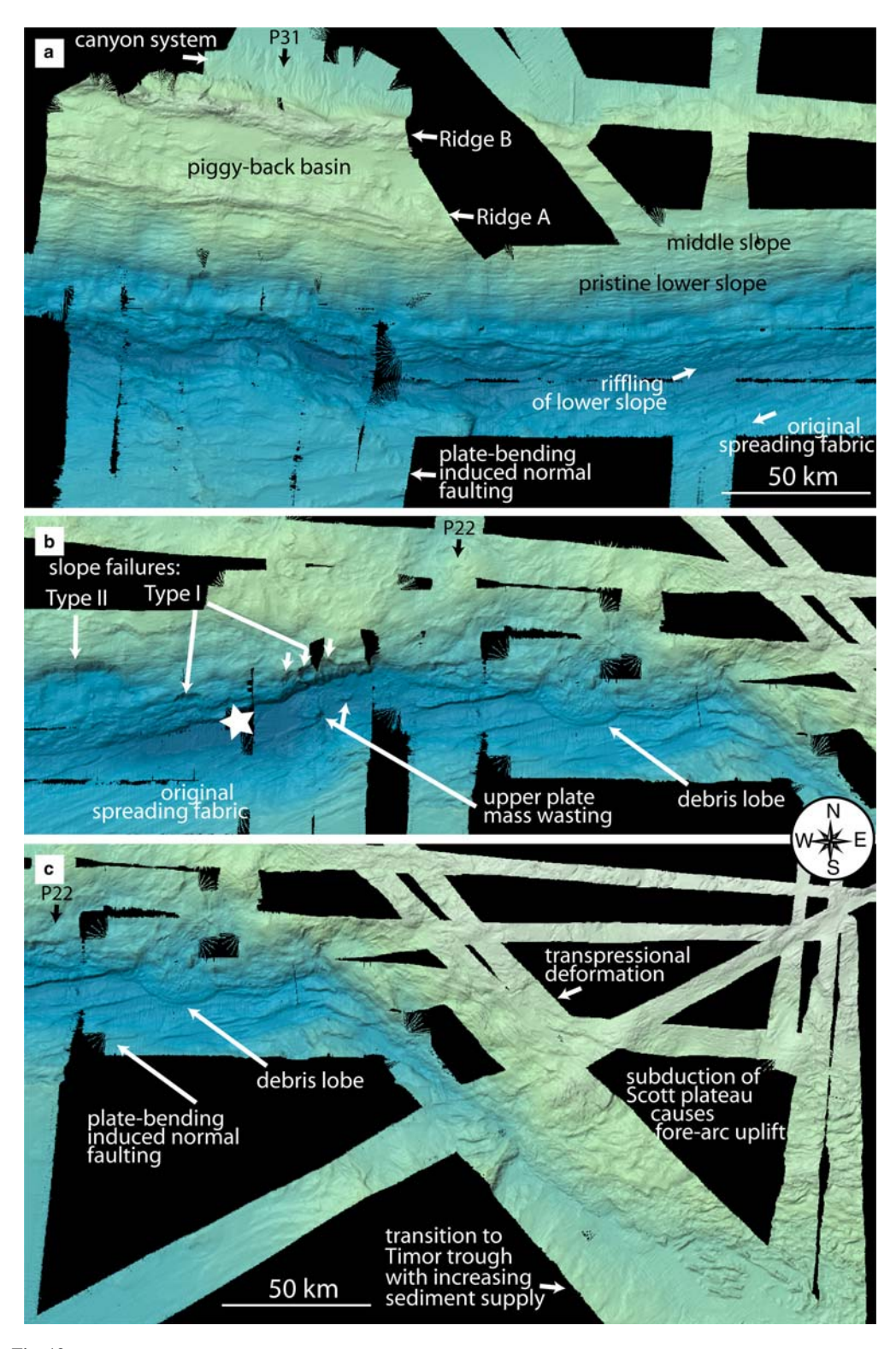


Fig. 13.

The deformation front is additionally affected by transpressional deformation related to the southward curvature of the trench as it merges into the Timor trough (Fig. 13c). The relocated epicentre of the 1977 earthquake (Engdahl & Villaseñor 2002) is shown in Figure 13b. The main event and the aftershock sequence likely resulted from slip along the re-activated inherited sea floor fault fabric as it bends underneath the upper plate and ruptures the oceanic lithosphere to a depth of 30–50 km (Spence 1986; Lynnes & Lay 1988).

One of the most prominent features on the wideangle profiles is the shallow upper plate mantle, which is found at a depth of c. 16 km underneath the fore-arc basin. The low seismic velocities of c. 7.5 km/s detected here (to c. 2 km below the Moho) are attributed to hydration and serpentinization of mantle peridotite (Faccenda et al. 2009), requiring faults to penetrate the oceanic crust and reach deep into the mantle. This is supported by the hypocentre relocation of the 1977 Sumba earthquake sequence, which resolved normal faulting to affect the oceanic lithosphere to a depth of 34 km (Spence 1986) as indicated above. The shallow position of the upper plate mantle may fundamentally affect seismogenesis along the Java margin as it limits the extent of the seismogenic zone. The interface contact with weak, hydrated minerals such as serpentinite, which mechanically cannot support stick-slip behaviour, would result in stable sliding downdip of the seismogenic zone (e.g. Hyndman et al. 1997; Oleskevich et al. 1999). However, exceptions to this concept may exist, for example offshore Sumatra, where earthquake nucleation has been proposed to occur in the mantle (Dessa et al. 2009; Klingelhoefer et al. 2010) or offshore Japan, where earthquake clusters below the depth of the fore-arc Moho are related to seamount detachment (Uchida et al. 2010). Along with the depth extent of the seismogenic zone, the size of the lateral rupture zone determines the potential magnitude of subduction thrust earthquake. Local asperities that may act as barriers to rupture thus will also influence the magnitude. The eastward propagating minimum 200 km rupture of the 1977 Sumba normal faulting event was likely limited by

the thick crust of the Scott plateau, acting as a barrier to further rupture propagation.

Remaining issues

The transition from oceanic subduction to the collisional regime along the Timor trough occurs south of Sumba Island (Fig. 13c), where the crystalline crust of the Sumba block is imaged in the tomographic model (Fig. 2, panel f). The easternmost profile is located east of Sumba Island around 121°E (Fig. 1) (Shulgin et al. 2009) and documents the early stages of continent-island arc collision along the westernmost extension of the Timor trough (Fig. 2g). The relative motion along this segment of the Timor trough has slowed to c. 15 mm/a. The incoming crust of the Scott plateau reaches a thickness of 15 km as it subducts below the fold-and-thrust belt of the upper plate. The increased sediment thickness is reflected in decreasing water depth in the trough (Fig. 13c). Sediments are likely sourced from the Australian continent and contribute to the evolution of a large accretionary body with a width of c. 130 km. This evolving collisional system is dominated by the Sumba Ridge, a high velocity block that acts as backstop to the accretionary prism in the south (Fig. 2, panel g). Backthrusting onto the Savu Basin in the north originates from the compressional deformation caused by the northward propagation of the Australian lithosphere (Bock et al. 2003).

Conclusions

This study investigates contrasting modes of deformation in three segments of the Java convergent margin, defined by varying processes of mass transfer. Sediment supply to the trench acts as the principal factor governing lower to upper plate material transfer. The decreasing sediment supply to the Java trench from west to east correlates with a changing pattern of mass flux: from sediment accretion offshore western Java to tectonic erosion off central Java. Sediment accretion characterizes the Sumatra sector of the Sunda margin, where sediment input on

Fig. 13. High-resolution bathymetric mapping offshore Lombok to Sumba. Location is indicated in Figure 3.

(a) The accretionary prism is dominated by two elongated ridges which host piggy-back basins. The topography of the lower plate is dominated by plate-bending induced normal faulting locally overprinted by original sea floor spreading fabric. Oceanic crust topography causes riffling of lower slope material upon subduction underneath the frontal prism. Mass wasting occurs to the fore-arc basin in the north. (b) Slope failure results in landslides affecting the lower slope (Type I failure) or the middle and lower slope (Type II failure). The headwall scarp of the Type II failure is offset northwards, indicating failure in successive phases. Three adjacent Type I slides are indicated and associated upper material wasting is observed on the trench floor. White star indicates hypocentre location of 1977 Sumba earthquake. (c) Transition to the Timor trough coincides with a shallowing of the sea floor and is associated with transpressional deformation and uplift of the overriding plate. A debris lobe is observed in the trench and will eventually be re-incorporated into the frontal prism. Refer to Figure 10 caption for additional display information.

the oceanic plate continuously increases to the north with closer proximity to the Ganges-Brahmaputra system (Moore et al. 1980). The western Java segment is characterized by a net addition of material from the lower plate to the upper plate and by an oceanic sea floor topography smoothed by a sediment apron. Offshore western Java, frontal sediment accretion dominates and c. 2/3 of the trench sediment sequence is incorporated into an imbricate thrust belt (Schlueter et al. 2002) (Figs 6 & 7). The thickness of material subducting beyond the frontal accretionary prism ranges from 500 to 1000 m per trench km here. Basal accretion likely occurs below the fore-arc high, contributing to the evolution and uplift of a > 100 km wide bivergent wedge (Fuller et al. 2006; Kopp et al. 2009).

To the east, offshore central Java, the transition from sediment accretion to tectonic erosion occurs over a distance of less than 100 km around 110°E (between profile P18 and P16 in Fig. 1). Here, the trench is devoid of sediments except for isolated sediment ponds (Masson et al. 1990). A complex canyon system traverses the continental slope and supplies material to the Java and Lombok fore-arc basins. Sediment discharged from Java and the Lesser Sunda islands does not reach the trench, but is trapped in the fore-arc basins as the distance from the trench to the active volcanic arc increases from west to east. The nature of the basement of the arc framework crust underneath the Java and Lombok fore-arc basins remains enigmatic. Based on previous work by Curray et al. (1977) and Kopp et al. (2002), it is proposed that the fore-arc crust could be composed of an altered oceanic terrane, which resisted subduction due to increased positive buoyancy (Planert et al. 2010). An alternative view is based on the rock record of Sumba Island: the seaward extent of continental crust south of Java and the Lesser Sunda islands could be the lateral continuation of the Late Cretaceous arc massif (Rutherford et al. 2001).

High relief oceanic basement is subducting offshore central and eastern Java, leading to a rough sea floor and causing frontal erosion of the fore-arc (Fig. 10). The margin geometry is influenced by the subduction of an oceanic plateau, the Roo Rise, underneath the Java fore-arc. The Nusa Tenggara segment offshore the Lesser Sunda islands experiences the transition from oceanic subduction to continent island arc collision (Fig. 13), with a rapid change in upper plate structure along strike

The eastern Sunda margin is prone to large potentially tsunamigenic landslides. Landslides are categorized in Type I and Type II slides, following the nomenclature of Yamada *et al.* (2010). Type I slides are of smaller dimension and occur on the lower slope, while Type II slides affect a larger

area/volume and are observed on the middle and upper slopes. Both types are triggered by the oversteepening of the slope either due to the subduction of relief or near a thrust surface in the frontal imbricate thrust fan (Fig. 13). While the smaller Type I slides are ubiquitous along the Java margin, the larger Type II slides are only observed in the easternmost segment. Brune et al. (2010b) have identified 12 landslides along the Sunda margin from high-resolution multibeam bathymetry. While the volume of the Type I landslides is typically less than 5 km³, the three largest ones, which are located in the transition zone from the Java trench to the Timor trough, show large volumes of 15-20 km³ and have originated on the middle slope, which qualifies them as Type II slides (Fig. 13b). A potential contribution of the Type II slides identified in the vicinity of the 1977 Sumba earthquake is not verified. Tsunami propagation modelling successfully predicted the observed run-up heights from the earthquake tsunami alone and does not necessarily require a further contribution from a landslide tsunami (Brune et al. 2010a).

An additional process for tsunami generation is the potential activation of splay faults during the co-seismic phase. Splay faults connect to the megathrust at depth and dip steeply to the surface, as imaged offshore western Java (Kopp *et al.* 2009) (Figs 6 & 7) and off the Lesser Sunda islands (Lueschen *et al.* 2010). Thus the low-angle slip of the megathrust will potentially be transferred to a higher angle, which may greatly enhance sea floor displacement (Tanioka & Satake 1996). Due to the lack of deeply penetrating multichannel seismic data, the role of potential splay faults in the generation of the 1994 and 2006 Java tsunamis remains unresolved.

Deep-seated subduction processes excerpt control on the structure and deformation of the upper plate as well as on the seismogenesis of the fore-arc. The most dramatic effects are observed in the central-eastern Java segment, where deformation of the sedimentary units in the fore-arc basin (Figs 7 & 11) and backthrusting of the fore-arc high onto the basin (Fig. 2, panels c, d) are documented. A decrease in the subduction angle of the underthrusting plate, as detected off South America, however, is not observed here (Koulakov et al. 2007). This concurs with results from numerical modelling, which predict that a moderate-sized plateau will not significantly alter the subduction angle (Gerya et al. 2009). In addition, the modelling also predicts that a decrease in magmatic activity is unlikely. Tomographic inversion has revealed the interplay between the fore-arc and the volcanism on Java, where the high vp/vs ratio of a pronounced low velocity anomaly in the Javanese crust is indicative of fluid

ascent from the underthrusting plate to the volcanic arc (Koulakov et al. 2007) and has been interpreted to image the related fluid ascending paths (Wagner et al. 2007). Other predictions based on numerical modelling regarding the fore-arc morphology are also matched: a local increase in topography is observed in the overriding plate as well as a northward displacement of the deformation front (Kopp et al. 2006), indicative of erosive processes here. Stress fluctuations govern erosion, which requires a strong subduction thrust fault and a mechanically weak overlying wedge. On short timescales, earthquakes are a common mechanism to cause variations of stress, which then occur from the interseismic phase to the co-seismic activity (Wang et al. 2010). Changes in basal fault strength may also be caused by the rough topography of an oceanic plate lacking a significant sediment cover. Deformation of the wedge caused by the impinging bathymetric features will mechanically weaken the prism, which is then overlying a strong basal detachment, providing conditions favouring subduction erosion.

Basal subduction erosion would pose a tectonic mechanism for basin subsidence; however, this would require the underthrusting plate to remain in contact with the upper plate from the trench to underneath the fore-arc basin. The tomographic images of Figure 2 clearly demonstrate that the underthrusting plate dips into the upper mantle beneath the outer fore-arc high. Further evidence for this configuration comes from earthquake hypocentres distribution (Wagner et al. 2007; Wittwer 2010) and gravity modelling (Grevemeyer & Tiwari 2006; Planert et al. 2010; Shulgin et al. 2010). In addition, satellite magnetic data record a significant anomaly extending seaward, resulting from a hydrated mantle wedge underneath the fore-arc (Blakely et al. 2005). This then raises the question if subduction erosion of the upper plate's lithospheric mantle wedge occurs and if this accomplishes basin subsidence. This issue, however, is beyond the scope of this paper.

Seismogenesis

The Java margin is characterized by a notable absence of Mw > 8 earthquakes compared to its Sumatran counterpart, leading to the question of what controls seismic rupture and consequently the potential size of earthquakes offshore Java. The magnitude of an earthquake is associated with the size of its rupture zone. Slip motion on a fault will depend on the tectonic environment of the source region (Bilek 2007). Two aspects are related to slip motion: (1) the role of the decollement zone and (2) the role of sea floor relief acting as asperities or barriers to rupture.

The notion that trench sediments affect seismogenesis was brought forward by Larry Ruff (Ruff 1989) and is here extended to the concept of the subduction channel in general. On a global scale, giant megathrust earthquakes (Mw > 8.5) are observed in systems characterized by sediment-flooded trenches [e.g. Sumatra (1883, 2004, 2005), Southern Chile (1960, 2010), Alaska/Aleutians (1964, 1965, 1986)] as well as at erosional margins [Kamchatka (1952), Kuril Islands (1963), Northern Chile (1868, 1877)], which show a subduction channel of several hundred metres in thickness. The existence and geometry (thickness) of a subduction channel thus influences rupture propagation to a greater degree than the nature of the material in it (trench sediment v. upper plate erosional debris) (Tanioka et al. 1997; Bilek & Lay 1999). A discussion on the role of fluids in this context, however, is beyond the scope of our data.

The second aspect regards sea floor roughness and the question of whether basement relief acts as an asperity or barrier to seismic rupture (Bilek & Lay 2002). Certainly this will not play a role where basement highs are deeply buried in the subduction channel. Here, subduction channel material smoothes sea floor relief and cushions upper plate contact. Where this is not the case, underthrusting seamounts or ridges may pose a limit to lateral rupture propagation, as do crustal faults (Collot et al. 2004). Bathymetric relief on the underthrusting plate will lead to variations in mechanical coupling and high friction models as well as low friction models have been proposed (Cloos 1992; Mochizuki et al. 2008). Large seamounts (>3 km height) may increase the normal stress between the plate and raise interplate coupling (Scholz & Small 1997). On the contrary, reduction of normal stress has been proposed to result from elevated pore pressure of entrained fluid-rich sediment during erosion (von Huene et al. 2004). Weak interplate coupling may be related to the damage caused by erosion that inhibits the accumulation of elastic strain energy (Mochizuki et al. 2008). Recurring Mw c. 7 earthquakes are related to seamount subduction in the Japan trench (Mochizuki *et al.* 2008) where weak coupling has been linked to fluid-rich sediment and migration of fluids at the base of the seamount.

Along the Java subduction zone, different tectonic features exert a first-order control on the seismogenesis of the margin and govern the lack of Mw > 8 megathrust earthquakes:

 Our tomographic images reveal a shallow upper plate Moho with low mantle velocities, indicative of hydrated minerals (Fig. 2). Hydration is caused by fluids, which are released from the subducting slab and

entrenched sediments, leading to serpentinization of the mantle wedge (Hyndman & Peacock 2003). The limited downdip extent of the seismogenic zone is also supported by gravity data and thermal modelling (Grevemeyer & Tiwari 2006) as well as by the fore-arc morphology (Krabbenhoeft *et al.* 2010).

In the central Java segment, seismic rupture would additionally be limited along strike by subducted basement relief acting as barriers that will resist co-seismic slip. Erosional damage related to seamount/Roo Rise plateau subduction may hinder the accumulation of elastic strain (Mochizuki et al. 2008). Local elevation in pore pressure of sediment entrained during underthrusting of a seamount may also be expected. The uneven slip distribution recorded during the co-seismic phases of the recurring tsunami earthquakes on this margin sector (Fig. 1) (Ammon et al. 2006; Bilek & Engdahl 2007) document the highly heterogeneous plate coupling of the fore-arc. The structural diversity of the underthrusting plate in conjunction with fluid-related processes governs the heterogeneous plate coupling offshore Java.

A heterogeneous structure has also been documented for the onshore portion of the upper plate fore-arc. Two high velocity, rigid blocks sandwich a low velocity anomaly in southern Java, which is interpreted as a weakened contact zone. The predominantly strike-slip focal mechanism of the Mw = 6.3 Java event in May of 2006 corresponds to the orientation of this contact zone (Wagner *et al.* 2007). However, our data lack the resolution to precisely determine the role of upper plate heterogeneity in seismic rupture propagation patterns.

In summary, the complex megathrust interface geometry is the main factor for the observed absence of large (>8) magnitude earthquakes offshore Java (Newcomb & McCann 1987), while smaller magnitude earthquakes frequently occur. The interplay between the tectonic habitat of the source region and the seismogenesis of large megathrust earthquakes is only crudely understood to date. The topic invites further research in the future to better understand the seismogenic segmentation and the specific geohazard potential of convergent plate boundaries.

I am indebted to numerous colleagues who have been involved in the Java margin studies. The concepts presented here have evolved from the many discussions with the members of my group at IFM-GEOMAR (D. Hindle, L. Planert, M. Scherwath, A. Shulgin, A. Wittwer, J. Zhu and M. Zillmer). The data acquisition would not have been possible without the enthusiastic

support of J. Bialas, A. Krabbenhoeft, C. Papenberg, J. Petersen, I. Trummer, D. Wagner. Special thanks go out to E. R. Flueh for his readiness to lead the cruises. W. Weinrebe is warmly thanked for processing of the multibeam data. The studies were conducted in collaboration with Y. Djajadihardja (BPPT Jakarta), B. Luehr and O. Oncken (GFZ Potsdam), C. Mueller, C. Gaedicke, C. Reichert (BGR Hannover), and W. Rabbel (CAU Kiel). This work would not have been possible without the continuous support of the SONNE program by the German Federal Ministry for Science and Technology BMBF. We are indebted to the captains and crews of RV SONNE for the excellent support and performance at sea. Cruises SO137, SO138, SO176, SO179 and SO190 were supported by grants 03G0137A (GINCO I), 03G0138A (GINCO II), 03GO176A (MERAMEX), 03G03G0190A and 03G0190B (SINDBAD project). Additional support was supplied by the DFG through the SUNDA project (grant KO2961/1-2) and by the GEOTECHNOLOGIEN program of BMBF and DFG for the SUNDAARC project (grant 03G0579B).

I thank reviewer D. Scholl for many discussions and thoughtful comments that greatly helped to improve the manuscript. Comments by an anonymous reviewer additionally tightened the manuscript. I kindly acknowledge volume editor R. Hall and M. Cottam for their editorial guidance.

References

- ABERCROMBIE, R., ANTOLIK, M., FELZER, K. & EKSTRÖM, G. 2001. The 1994 Java tsunami earthquake: slip over a subducting seamount. *Journal of Geophysical Research*, **106**, 6595–6607.
- Ammon, C. J., Kanamori, H., Lay, T. & Velasco, A. A. 2006. The 17 July 2006 Java tsunami earthquake. Geophysical Research Letters, 33, L24308, doi: 10.1029/2006GL028005.
- AUDLEY-CHARLES, M. G. 1975. The Sumba fracture: a major discontinuity between eastern and western Indonesia. *Tectonophysics*, **26**, 213–228.
- AUDLEY-CHARLES, M. G. 2004. Ocean trench blocked and obliterated by Banda forearc collision with Australian proximal continental slope. *Tectonophysics*, **389**, 65–79
- BABA, T., HORI, T. *ET AL.* 2001. Deformation of a seamount subducting beneath an accretionary prism: constraints from numerical simulation. *Geophysical Research Letters*, **28**, 1827–1830.
- BEIERSDORF, H. 1999. Geoscientific investigations at the active convergence zone between the eastern Eurasian and Indo-Australian plates off Indonesia. BGR Cruise Report SO139 GINCO 3.
- BIALAS, J. & FLUEH, E. R. 1999. Ocean bottom seismometers. *Sea Technology*, **40**, 41–46.
- BILEK, S. 2007. Influence of subducting topography on earthquake rupture. *In*: DIXON, T. & MOORE, J. C. (eds) *The Seismogenic Zone of Subduction Thrust Faults*. Columbia University Press, Columbia, 123–146.
- BILEK, S. & ENGDAHL, R. 2007. Rupture characterization and aftershock relocations for the 1994 and 2006 tsunami earthquakes in the Java subduction zone. *Geophysical Research Letters*, **34**, doi: 10.1029/2007GL031357.

- BILEK, S. & LAY, T. 1999. Rigidity variations with depth along interplate megathrust faults in subduction zones. *Nature*, 400, 443–446.
- BILEK, S. & LAY, T. 2002. Tsunami earthquakes possibly widespread manifestations of frictional conditional stability. *Geophysical Research Letters*, 29, 14, doi: 10.1029/2002GL015215.
- BLAKELY, R. J., BROCHER, T. M. & WELLS, R. E. 2005. Subduction-zone magnetic anomalies and implications for hydrated forearc mantle. *Geology*, 33, 445–448.
- BOCK, Y., PRAWIRODIRDJO, L. ET AL. 2003. Crustal motion in Indonesia from Global Positioning System measurements. Journal of Geophysical Research, 108, 2367, doi: 10.1029/2001JB000324.
- BRUNE, S., LADAGE, S., BABEYKO, A. Y., MÜLLER, C., KOPP, H. & SOBOLEV, S. V. 2010a. Submarine landslides at the eastern Sunda margin: observations and tsunami impact assessment. *Natural Hazards*, doi: 10.1007/s11069-009-9487-8.
- BRUNE, S., BABEYKO, A. Y., LADAGE, S. & SOBOLOEV, S. V. 2010b. Landslide tsunami hazard in the Indonesian Sunda Arc. Natural Hazards and Earth System Sciences, 10, 589–604.
- CLOOS, M. 1992. Thrust-type subduction zone earthquakes and seamount asperities: a physical model for earthquake rupture. *Geology*, 20, 601–604.
- COLLOT, J.-Y., MARCAILLOU, B. ET AL. 2004. Are rupture zone limits of great subduction earthquakes controlled by upper plate structures? Evidence from multichannel seismic reflection data acquired across the northern Ecuador-southwest Colombia margin. *Journal of Geo*physical Research, 109, doi: 10.1029/2004JB003060.
- CURRAY, J. R., SHOR, G. S., RAITT, R. W. & HENRY, M. 1977. Seismic refraction and reflection studies of crustal structure of the Eastern Sunda and Western Banda Arcs. *Journal of Geophysical Research*, 82, 2479–2489.
- DARDJI, N., VILLEMIN, T. & RAMPNOUS, J. P. 1994. Paleostress and strike-slip movement: the Cimandiri fault zone, west Java, Indonesia. *Journal of SE Asian Earth Sciences*, 9, 3–11.
- DESSA, J.-X., KLINGELHOEFER, F. ET AL. & THE SUMATRA-OBS SCIENCE TEAM. 2009. Megathrust earthquakes can nucleate in the forearc mantle: evidence from the 2004 Sumatra event. Geology, 37, doi: 10.1130/G25653A.1.
- DIAMENT, M., HARJONO, H. ET AL. 1992. Mentawai fault zone off Sumatra: a new key to the geodynamics of western Indonesia. *Geology*, **20**, 259–262, doi: 10.1130/0091-7613(1992)020<0259:MFZOSA>2.3. CO:2.
- DOMINGUEZ, S., MALAVIEILLE, J. & LALLEMAND, S. E. 2000. Deformation of accretionary wedges in response to seamount subduction: insights from sandbox experiments. *Tectonics*, 19, 1, doi: 10.1029/1999TC900055.
- ENGDAHL, E. R. & VILLASEÑOR, A. 2000. Global Seismicity: 1900–1999. *In*: Lee, W. H. K., Kanamori, H., Jennings, P. C. & Kisslinger, C. (eds) *International Handbook of Earthquake and Engineering Seismology, Part A.* Academic Press, London, 665–690.
- FACCENDA, M., TARAS, T. V. & BURLINI, L. 2009. Deep slab hydration induced by bending-related variations in tectonic pressure. *Nature Geoscience*, 2, 790–793, doi: 10.1038/ngeo656.

- FISHER, D., GARDNER, T., SAK, P., SANCHEZ, J., MURPHY, K. & VANNUCCHI, P. 2004. Active thrusting in the inner forearc of an erosive convergent margin, Pacific coast, Costa Rica. *Tectonics*, 23, doi: 10.1029/2002TC001464.
- FONT, Y. & LALLEMAND, S. 2009. Subducting oceanic high causes compressional faulting in southernmost Ryukyu forearc as revealed by hypocentral determinations of earthquakes and reflection/refraction seismic data. *Tectonophysics*, 466, doi: 10.1016/ j.tecto.2007.11.018.
- Fritz, H., Kongko, W. *Et al.* 2007. Extreme run-up from the 17 July 2006 Java tsunami. *Geophysical Research Letters*, **34**, doi: 10.1029/2007GL029404.
- FULLER, C. W., WILLET, S. D., FISHER, D. & LU, C. Y. 2006. A thermomechanical wedge model of Taiwan constrained by fission-track thermochronometry. *Tectonophysics*, 425, doi: 10.1016/j.tecto.2006.05.018.
- GERYA, T. V., FOSSATI, D., CANTIENI, C. & SEWARD, D. 2009. Dynamic effects of aseismic ridge subduction: numerical modeling. *European Journal of Mineralogy*, 21, doi: 10.1127/0935-1221/2009/0021-1931.
- Grevemeyer, I. & Tiwari, T. M. 2006. Overriding plate controls spatial distribution of megathrust earthquakes in the Sunda-Andaman subduction zone. *Earth and Planetary Science Letters*, **251**, 199–208.
- Gutscher, M.-A., Kukowski, N., Malavieille, J. & Lallemand, S. 1998. Episodic imbricate thrusting and underthrusting: analog experiments and mechanical analysis applied to the Alaskan accretionary wedge. *Journal of Geophysical Research*, **103**, 10 161–10 176.
- HALL, R. & SMYTH, H. R. 2008. Cenozoic arc processes in Indonesia: identification of the key influences on the stratigraphic record in active volcanic arcs. *Geological Society of America Special Paper*, 436, 27–54.
- HAMILTON, W. 1979. Tectonics of the Indonesian Region. U.S. Geological Survey Professional Paper, 1078
- HEINE, C., MUELLER, R. D. & GAINA, C. 2004. Reconstructing the lost Tethys Ocean basin: convergence history of the SE Asian margin and marrine gateways.
 In: CLIFT, P., HAYES, D., KUHNT, W. & PINXIAN, W. (eds) Continent-Ocean Interactions Within East Asian Marginal Seas. American Geophysical Union, Washington DC, Geophysical Monograph Series, 149, 37–54.
- HEIRTZLER, J. R., VEEVERS, J. J. ET AL. 1974. Site 261. Initial Reports of DSDP, 27, 129–192.
- HUCHON, P. & LE PICHON, X. 1984. Sunda strait and central Sumatra fault. *Geology*, **12**, 668–672.
- HYNDMAN, R. D. & PEACOCK, S. M. 2003. Serpentinization of the forearc mantle. Earth and Planetary Science Letters, 212, 417–432.
- HYNDMAN, R. D., YAMANO, M. & OLESKEVICH, D. A. 1997. The seismogenic zone of subduction thrust faults. *Island Arc*, **6**, 3, doi: 10.1111/j.1440-1738.1997.tb00175.x.
- ISOZAKI, Y., MARUYAMA, S. & FURUOKA, F. 1990. Accreted oceanic materials in Japan. *Tectonophysics*, 181, 171–205.
- KANAMORI, H. 1972. Mechanism of tsunami earthquakes. Physics of the Earth and Planetary Interiors, 6, 346–359.

KATO, K. & TSUJI, Y. 1995. Tusnami of the Sumba earthquake of August 19, 1977. *Journal of Natural Disaster Sciences*, 17, 87–100.

- KLINGELHOEFER, F., GUTSCHER, M.-A. *ET Al.* 2010. Limits of the seismogenic zone in the epicentral region of the 26 December 2004 great Sumatra—Andaman earthquake: results from seismic refraction and wide-angle reflection surveys and thermal modelling. *Journal of Geophysical Research*, **115**, B01304, doi: 10.1029/2009JB006569.
- KOPP, H. & KUKOWSKI, N. 2003. Backstop geometry and accretionary mechanics of the Sunda margin. *Tectonics*, 22, doi: 10.1029/2002TC001420.
- KOPP, H., FLUEH, E. R., KLAESCHEN, D., BIALAS, J. & REICHERT, C. 2001. Crustal structure of the central Sunda margin at the onset of oblique subduction. *Geophysical Journal International*, **147**, 449–474, doi: 10.1046/j.0956-540x.2001.01547.x.
- KOPP, H., KLAESCHEN, D., FLUEH, E. R. & BIALAS, J. 2002. Crustal structure of the Java margin from seismic wide-angle and multichannel reflection data. *Journal of Geophysical Research*, 197, doi: 10.1029/ 2000JB000009.
- KOPP, H., FLUEH, E. R., PETERSEN, C. J., WEINREBE, W., WITTWER, A. & MERAMEX SCIENTISTS. 2006. The Java margin revisited: evidence for subduction erosion off Java. *Earth and Planetary Science Letters*, 242, 130–142, doi: 10.1016/j.epsl.2005. 11.036.
- KOPP, H., WEINREBE, W. ET AL. 2008. Lower slope morphology of the Sumatra trench system. Basin Research, doi: 10.1111/j.1365-2117.2008.00381.x.
- KOPP, H., HINDLE, D., KLAESCHEN, D., ONCKEN, O., REICHERT, C. & SCHOLL, D. 2009. Anatomy of the western Java plate interface from depth-migrated seismic images. *Earth and Planetary Science Letters*, doi: 10.1016/j.epsl.2009.09.043.
- KOULAKOV, I., BOHM, M. *ET Al.* 2007. P and S velocity structure of the crust and upper mantle beneath central Java from local tomography inversion. *Journal of Geophysical Research*, **112**, doi: 10.1029/2006JB004712.
- Krabbenhoeft, A., Weinrebe, W. *et al.* 2010. Bathymetry of the Indonesian Sunda margin relating morphological features of the upper plate slopes to the location and extent of the seismogenic zone. *Natural Hazards and Earth System Sciences*, **10**, 1899–1911, doi: 10.5194/nhess-10-1899-2010.
- Lelgemann, H., Gutscher, M.-A., Bialas, J., Flueh, E. R., Weinrebe, W. & Reichert, C. 2000. Transtensional basins in the western Sunda Strait. *Geophysical Research Letters*, **27**, 3545–3548.
- LITCHFIELD, N., ELLIS, S., BERRYMAN, K. & NICOL, A. 2007. Insights into subduction-related uplift along the Hikurangi Margin, New Zealand, using numerical modelling. *Journal of Geophysical Research*, 112, doi: 10.1029/2006JF000535.
- LUESCHEN, E., MUELLER, C. ET AL. 2010. Structure, evolution and tectonic activity at the Eastern Sunda forearc, Indonesia, from marine seismic investigations. *Tectonophysics*, doi: 10.1016/j.tecto.2010.06.008.
- LYNNES, C. & LAY, T. 1988. Source process of the Great Sumba Earthquake. *Journal of Geophysical Research*, 93, 13 407–13 420.

- MALOD, J. A. & KEMAL, B. M. 1996. The Sumatra margin: Oblique subduction and lateral displacement of the accretionary prism. *In:* HALL, R. & BLUNDELL, D. (eds) *Tectonic Evolution of South-East Asia*. Geological Society, London, Special Publications, **106**, 19–28.
- MALOD, J. A., KARTA, K., BESLIER, M. O. & ZEN, M. T., Jr. 1995. From normal to oblique subduction: Tectonic relationships between Java and Sumatra. *Journal of Souteast Asian Earth Sciences*, 12, 85–93.
- Masson, D. G. 1991. Fault patterns at outer trench walls. *Marine Geophysical Research*, 3, 13 209–13 225.
- MASSON, D. G., PARSON, L. M., MILSOM, J., NICHOLS, G., SIKUMBANG, N., DWIYANTO, B. & KALLAGHER, H. 1990. Subduction of seamounts at the Java Trench: a view with long-range sidescan sonar. *Tectonophysics*, 185, 18 551–18 565.
- MOCHIZUKI, K., YAMADA, T., SHINOHARA, M., YAMANAKA, Y. & KANAZAWA, T. 2008. Weak interplate coupling by seamounts and repeating M∼7 Earthquakes. *Science*, **321**, 1194–1197, doi: 10.1126/science.1160250.
- MOORE, G. F., CURRAY, J. R., MOORE, D. G. & KARIG, D. E. 1980. Variations in geologic structure along the Sunda Fore Arc, northeastern Indian Ocean. In: HAYS, D. E. (ed.) The Tectonic and Geologic Evolution of Southeast Asian Seas and Islands. American Geophysical Union, Washington DC, Geophysical Monograph Series, 23, 145–160.
- Mueller, C. & Neben, S. 2006. Seismic and geoacoustic investigations along the Sunda-Banda Arc transition. BGR Cruise Report SO190 Leg 1.
- MUELLER, C., KOPP, H. *ET AL.* 2008. From subduction to collision: The Sunda-Banda Arc transition. *EOS Transactions*, **89**, 49–60.
- MUELLER, R. D., ROEST, W. R., ROYER, J.-Y., GAHAGAN, L. M. & SCLATER, J. G. 1997. Digital isochrons of the world's ocean floor. *Journal of Geophysical Research*, **102**, 3211–3214.
- Newcomb, K. R. & McCann, W. R. 1987. Seismic history and seismotectonics of the Sunda Arc. *Journal of Geophysical Research*, **92**, 421–439.
- OLESKEVICH, D. A., HYNDMAN, R. D. & WANG, K. 1999. The updip and downdip limits to great subduction earthquakes: Thermal and structural models of Cascadia, south Alaska, SW Japan, and Chile. *Journal of Geophysical Research*, **104**, 14 965–14 991.
- PLANERT, L., KOPP, H. ET AL. 2010. Lower plate structure and upper plate deformational segmentation at the Sunda-Banda arc transition, Indonesia. *Journal of Geo*physical Research, 115, doi: 10.1029/2009JB006713.
- Polet, J. & Thio, H. K. 2003. The 1994 Java tsunami earthquake and its 'normal' aftershocks. *Geophysical Research Letters*, **30**, 9, doi: 10.1029/2002GL016806.
- RUFF, L. 1989. Do trench sediments affect great earthquake occurrence in subduction zones? *Pageoph*, **129**, 262–282.
- RUTHERFORD, E., BURKE, K. & LYTWYN, J. 2001. Tectonic history of Sumba Island, Indonesia, since the late cretaceous and its rapid escape into the forearc in the Miocene. *Journal of Asian Earth Sciences*, 19, 453–479
- Schiller, D. M., Garrad, R. & Prasetyo, L. 1991. Eocene submarine fan sedimentation in southwest

- Java. *In: Proceedings of IPA 20th Anniversary Conference*. Indonesian Petroleum Association, Jakarta, 125–181.
- SCHLUETER, H. U., GAEDICKE, C. ET AL. 2002. Tectonic features of the southern Sumatra-western Java forearc of Indonesia. Tectonics, 21, doi: 10.1029/ 2001TC901048.
- SCHOLZ, C. & SMALL, C. 1997. The effect of seamount subduction on seismic coupling. *Geology*, **25**, 487–490.
- SHULGIN, A., KOPP, H. ET AL. 2009. Sunda-Banda arc transition: Incipient continent-island arc collision (northwest Australia). Geophysical Research Letters, 36, L10304, doi: 10.1029/2009GL037533.
- SHULGIN, A., KOPP, H. *ET AL*. 2011. Structural architecture of oceanic plateau subduction offshore Eastern Java and the potential implications for geohazards. *Geophysical Journal International*, **184**, 12–18, doi: 10.1111/j.1365-246x.2010.04834.x.
- SIMONS, W. J. F., SOCQUET, A. ET AL. 2007. A decade of GPS in Southeast Asia: resolving Sundaland motion and boundaries. *Journal of Geophysical Research*, 112, B06420, doi: 10.1029/2005JB003868.
- SMITH, W. H. F. & SANDWELL, D. T. 1997. Global seafloor topography from satellite altimetry and ship depth soundings. *Science*, 277, 1957–1962.
- Spence, W. 1986. The 1977 Sumba earthquake series: Evidence for slab pull force acting at a subduction zone. *Journal of Geophysical Research*, **91**, 7225–7329.
- SUKAMTO, R. 1975. Geologic map of Ujung Pandang, Indonesia. Direktorat Geologi. Bandung.
- SUSILOHADI, S., GAEDICKE, C. & ERHARDT, A. 2005. Neogene structures and sedimentation history along the Sunda forearc basins off southwest Sumatra and southwest Java. *Marine Geology*, 219, doi: 10.1016/ j.margeo.2005.05.001.
- Tanioka, Y., Ruff, L. & Satake, K. 1997. What controls the lateral variation of large earthquake occurrence along the Japan Trench? *Island Arc*, **6**, 261–266, doi: 10.1111/j.1440-1738.1997.tb00176.x.
- TANIOKA, Y. & SATAKE, K. 1996. Tsunami generation by horizontal displacement of ocean bottom. *Geophysical Research Letters*, 23, 861–864.
- TAYLOR, F. W., BEVIS, M. G. ET AL. 1995. Geodetic measurements of convergence at the new hebrides island arc indicate arc fragmentation due to an impinging aseismic ridge. Geology, 23, 1011–1014.
- TAYLOR, F. W., MANN, P. ET AL. 2005. Rapid forearc uplift and subsidence caused by impinging bathymetric features: Examples from the new hebrides and solomon arcs. *Tectonics*, 24, TC6005, doi: 10.1029/ 2004TC001650.
- TREGONING, P., BRUNNER, F. K. ET AL. 1994. First geodetic measurement of convergence across the Java Trench. Geophysical Research Letters, 21, 2135–2138.

- UCHIDA, N., KIRBY, S., OKADA, T., HINO, R. & HASEGAWA, A. 2010. Supraslab earthquake clusters above the subduction plate boundary offshore Sanriku, northeastern Japan: seismogenesis in a graveyard of detached seamounts? *Journal of Geophysical Research*, 115, doi: 10.1029/2009JB006797.
- VAN HUNEN, J., VAN DEN BERG, A. P. & VLAAR, N. J. 2002. On the role of subducting oceanic plateaus in the development of shallow flat subduction. *Tectonophysics*, 352, 317–333.
- von Huene, R. 2008. When seamounts subduct. *Science*, doi: 10.1126/science.1162868.
- VON HUENE, R. & RANERO, C. R. 2003. Subduction erosion and basal friction along the sediment-starved convergent margin off Antofagasta, Chile. *Journal* of *Geophysical Research*, 108, doi: 10.1029/ 2001JB001569.
- VON HUENE, R., RANERO, C. R. & WEINREBE, W. 2000. Quaternary convergent margin tectonics of Costa Rica, segmentation of the Cocos plate, and Central American volcanism. *Tectonics*, 19, 314–334.
- von Huene, R., Ranero, C. & Vannucchi, P. 2004. Generic model of subduction erosion. *Geology*, **32**, 913–916, doi: 10.1130/G20563.1.
- VON HUENE, R., RANERO, C. & SCHOLL, D. 2009. Convergent margin structure in high-quality geophysical images and current kinematic and dynamic models. In: LALLEMAND, S. & FUNICIELLO, F. (eds) Subduction Zone Geodynamics. Springer, Berlin, 137–157; doi: 10.1007/978-3-540-87974-9.
- WAGNER, D., KOULAKOV, I. ET AL. & MERAMEX SCIENTISTS 2007. Joint inversion of active and passive seismic data in Central Java. Geophysical Journal International, 170, doi: 10.1111/j.1365-246X.2007.03435.x.
- WANG, K. & Hu, Y. 2006. Accretionary prisms in subduction earthquake cycles: the theory of dynamic Coulomb wedge. *Journal of Geophysical Research*, 111, B06410, doi: 10.1029/2005JB004094.
- WANG, K., Hu, Y., VON HUENE, R. & KUKOWSKI, N. 2010. Interplate earthquakes as a driver of shallow subduction erosion. *Geology*, **38**, 431–434.
- WERNER, R., HAUFF, F. & HOERNLE, K. 2009. SO-199 CHRISP: Christmas Island Seamount Province and the Investigator Ridge: age and causes of intraplate volcanism and geodynamic evolution of the south-eastern Indian Ocean. IFM-GEOMAR Report, 25.
- WITTWER, A. 2010. Crustal and upper mantle structure of the central Java subduction zone from marine wideangle seismics. PhD thesis, University of Kiel.
- YAMADA, Y., YAMASHITA, Y. & YAMAMOTO, Y. 2010. Submarine landslides at subduction margins: insights from physical models. *Tectonophysics*, 484, doi: 10.1016/j.tecto.2009.09.007.